Active Yaw Rate Stabilization for Steer-by-Wire Cars

Master's thesis in Systems, Control and Mechatronics

Mohammad Faddawi
Elmer Janmark

DEPARTMENT OF MECHANICS AND MARITIME SCIENCES

CHALMERS UNIVERSITY OF TECHNOLOGY
Gothenburg, Sweden 2026
www.chalmers.se

Master's thesis 2026

Active Yaw Rate Stabilization for Steer-by-Wire Cars

Mohammad Faddawi
Elmer Janmark

Department of Mechanics and Maritime Sciences
Vehicle Engineering and Autonomous Systems
Vehicle Dynamics
Chalmers University of Technology
Gothenburg, Sweden 2026

Active Yaw Rate Stabilization for Steer-by-Wire Cars
Mohammad Faddawi
Elmer Janmark

Supervisor: Matthijs Klomp, Volvo Cars
Examiner: Fredrik Bruzelius, Department

Master's Thesis 2026
Department of Mechanics and Maritime Sciences
Vehicle Engineering and Autonomous Systems
Vehicle Dynamics
Chalmers University of Technology
SE-412 96 Gothenburg
Telephone +46 31 772 1000

Cover: A picture of the same car model used in this thesis project.

Typeset in LaTeX
Printed by Chalmers Reproservice
Gothenburg, Sweden 2026

Active Yaw Rate Stabilization for Steer-by-Wire Cars

Mohammad Faddawi
Elmer Janmark
Department of Mechanics and Maritime Sciences
Chalmers University of Technology

Abstract

The automotive industry is transitioning toward Steer-by-Wire (SbW) technology, which eliminates the traditional mechanical connection between the steering wheel and the road wheels. While a baseline SbW system actively controls the steering rack position based on driver input, the vehicle's overall lateral dynamics can lack sufficient damping to naturally reject macroscopic body disturbances, such as crosswinds or trailer sway.

This thesis develops and physically validates a closed-loop active lateral stabilization system that utilizes the SbW actuator as a continuous yaw rate correction channel. An ideal, undisturbed vehicle response is established using a linear single-track reference model. Against strict hardware constraints specifically a 50 ms actuation delay. A model-free Proportional (P) controller proved superior to model-based alternatives, guaranteeing absolute stability and preventing the delay-induced oscillations that arose with more complex algorithms.

Dynamic track testing in the prototype vehicle, including lane changes, trailer towing and subjective evaluation. The tests both objectively and subjectively confirmed that the active controller significantly improved disturbance attenuation without corrupting the driver's intended trajectory by reducing the yaw rate error, increasing responsiveness and improving stabilization compared to the unassisted vehicle. The feedback controller also demonstrated robust reference tracking despite unmodeled physical parameter variations, such as changes in tires and shifts in mass distribution, without requiring real-time system recalibration.

Keywords: SbW, Yaw Rate Control, Lateral Vehicle Dynamics, Disturbance Attenuation, Proportional Control, Grey-Box System Identification, Linear Single-Track Model, Vehicle Testing

Acknowledgements

First, We would like to express our gratitude to our supervisor Matthijs Klomp at Volvo Cars for his support, continuous guidance and for making this thesis much more enjoyable. He has been a great supervisor guiding us with his deep knowledge about vehicle dynamics and always brightening up the mood.
Furthermore we would like to thank Lidong Wang and Fredrik Bruzelius for their support, guiding us with the structure and writing of the thesis. We would also thank Volvo Cars for the opportunity and the resources they provided to carry out this thesis.

Mohammad Faddawi & Elmer Janmark, Gothenburg, June 2026

List of Acronyms

Below is the list of acronyms that have been used throughout this thesis, listed in alphabetical order:

SbW	Steer by Wire
ECU	Electronic Control Unit
IMU	Inertial Measurement Unit
CoG	Center of Gravity
LQR	Linear Quadratic Regulator
MB	Model-Based
RMS	Root Mean Square
NRMSE	Normalized Root Mean Square Error
ISO	International Organization for Standardization
PSD	Power Spectral Density
ESC	Electronic Stability Control
DOF	Degrees of Freedom

Nomenclature

Below is the nomenclature of parameters and variables that have been used throughout this thesis.

Parameters

A, B	State-space system matrices
C_f, C_r	Effective cornering stiffness of front and rear tires
I_z	Vehicle yaw moment of inertia
K	Optimal state-feedback gain matrix
K_d	Derivative gain
K_i	Integral gain
K_p	Proportional gain
K_{us}	Understeer gradient
L	Vehicle wheelbase ($L = l_f + l_r$)
l_f, l_r	Distances from the center of gravity to the front and rear axles
m	Vehicle mass
Q, R	LQR weighting matrices

Variables

a_y	Lateral acceleration
β	Vehicle side slip angle
δ	Front Road Wheels angle
δ_{driver}	Driver's steering wheel angle
δ_{add}	Corrective steering overlay angle
$e(t)$	Yaw rate tracking error
ψ	Yaw angle

r	Yaw rate ($\dot{\psi}$)
r_{ref}	Reference yaw rate
u	Control input vector
v_x	Longitudinal velocity
v_y	Lateral velocity
R_c	Turn Radius
x	State vector
F_f, F_r	Tire forces generated at the front and rear axles
M_z	Moment around z-axis
α_f, α_r	Front and Rear tire slip angles
R^2	coefficient of determination
$\hat{\Phi}$	Spectral Density
γ^2	Coherence Function
G	Transfer Function
G_{ss}	Steady State Gain
S	Sensitivity Function
M_s	The maximum amplitude ratio (peak gain) of the Sensitivity Function
$L(s)$	Open Loop Transfer Function
ω_{gc}, ω_{pc}	Gain and phase crossover frequencies.

Contents

1 Introduction

The automotive industry is undergoing a significant transformation driven by electrification, automation and the transition toward software defined vehicles. As a result, Steer-by-Wire (SbW) systems are being increasingly considered and represent a critical step in this evolution. The technology eliminates the mechanical connection between the steering wheel and the road wheels. While this decoupling offers unprecedented flexibility in steering feel and cabin design, it also fundamentally alters how the vehicle responds to external disturbances, creating new challenges and opportunities for active yaw control.

1.1 Background

In a conventional vehicle, the mechanical steering column provides a direct physical link between the driver and the road. When the vehicle encounters a disturbance, the forces are transmitted back to the driver, who naturally provides adjusted steering inputs to compensate.

A SbW system can filter out high frequency disturbances acting directly on the road wheels, such as the "kickback" experienced when hitting a pothole or a curbstone. Because the steering wheel and the steering column are mechanically decoupled, these road-level forces do not reach the driver, resulting in a smoother driving experience. However, current SbW systems often operate with an open-loop control configuration regarding the vehicle's yaw dynamics. The driver inputs a steering angle and the actuators position the wheels accordingly. As highlighted by Mortazavizadeh [1], these current open-loop architectures lack the intrinsic ability to reject external disturbances acting on the vehicle body, such as aerodynamic forces (e.g., crosswinds) or inertial effects.

In traditional vehicle architectures, significant deviations in yaw-rate caused by such disturbances are typically addressed through brake-based Electronic Stability Control (ESC). While highly effective in preventing loss of control, these interventions are triggering only when specific stability thresholds are exceeded. The mechanical decoupling provided by SbW systems unlocks the ability to use additional control inputs beyond the steering wheel angle. This introduces the opportunity to use active steering actuation to provide earlier and smoother yaw-rate corrections, shaping the vehicle's response seamlessly before brake-based interventions become necessary.

To mitigate these path deviations and enhance both safety and comfort, active lateral stabilization is required. calculated angle overlay can be applied to SbW systems, adding to the drivers steering input, enhancing stability while preserving the nominal steering behaviour and overall driving comfort.

1.2 Aim

The primary objective of this thesis is to design, implement and validate a closed-loop yaw stabilization system for a SbW prototype vehicle. The system aims to utilize yaw rate feedback to minimize the difference between a theoretically ideal vehicle response and the actual measured vehicle motion, actively attenuating the effect of external body level disturbances through a corrective steering overlay angle (δ_{add}).

Specifically, the project aims to develop and validate a controller capable of generating this corrective overlay under the hardware constraints of the prototype vehicle. Furthermore, the project investigates what control architecture is most suitable for this application by evaluating both classical PID components and optimal state feedback through LQR.

1.3 Limitations

To ensure the project remains focused and achievable within the time frame, the following limitations have been established

- The vehicle is modeled using a linear single track model. The purpose of this model is to generate the ideal, undisturbed reference yaw rate (r_{ref}) that the closed-loop controller aims to track. Which means dynamics such as roll, pitch and lateral load transfer are not considered.
- This project is limited to the linear handling dynamics of the vehicle. The reference models and control strategies will be designed for and validated within a lateral acceleration range $a_y < 5m/s^2$.

There are also constraints in the physical prototype vehicle and are independent of the project scope decisions

- The implementation is limited to the specific SbW prototype vehicle provided. The overlay steering action is restricted to a maximum of $\pm 7°$ on the road wheel angle and a signal resolution inherent to the CAN bus and actuation hardware in steps of 0.056 degrees.
- The hardware suffer from total identified system actuation delay of 50 ms, comprising the physical plant transport lag and communication latency. This delay was quantified by measuring the time elapsed between the transmission of a steering angle request and its physical execution, as recorded on the CAN bus.

1.4 Research Questions

This thesis seeks to answer the following primary research questions

- Can a simplified linear reference model provide a sufficient control target for closed-loop yaw rate stabilization and how does this linear constraint affect the driving experience during disturbances?
- What control architecture is most suitable for active yaw rate stabilization in a SbW system, subject to hardware delay?
- How effectively does the closed-loop SbW controller suppress external lateral disturbances in full-scale vehicle testing and to what extent does its performance remain robust when the physical vehicle deviates from the conditions assumed by the linear reference model?

2 Methodology

This chapter presents the theory and the practical approaches that form the foundation of this thesis. It covers the mathematical modeling of the vehicle's lateral dynamics, the principles of system identification used to estimate unknown vehicle parameters, the metrics used to validate the model and the control strategy implementation.

2.1 Vehicle Dynamics and System Modelling

To design and evaluate a steering controller without relying exclusively on physical track testing, a mathematical representation of the vehicle is required. In this section, a linear single-track model is derived, which provides the foundational state-space equations used later for both simulation and the reference target for the physical controller.

The mathematical formulation throughout this thesis is based on the work by Rajamani [2]. This model is extensively utilized in both academia and the automotive industry due to its optimal balance between simplicity and predictive accuracy for lateral handling analysis.

As detailed in this framework, the model simplifies the physical vehicle by combining the left and right wheels together into single units at the front and rear axles. It incorporates two degrees of freedom: the lateral translational motion (represented by the side slip angle, β) and the rotational motion around the vertical axis (represented by the yaw rate, r).

The derivation of the model relies on the assumption of linear vehicle behavior, specifically the linear tire approximation where the lateral tire force is directly proportional to the tire slip angle. This assumption remains highly accurate for standard driving maneuvers operating within the linear handling region. By applying Newton's and Euler's second laws of motion under these assumptions, the continuous state space equations governing the vehicle's lateral dynamics can be derived.

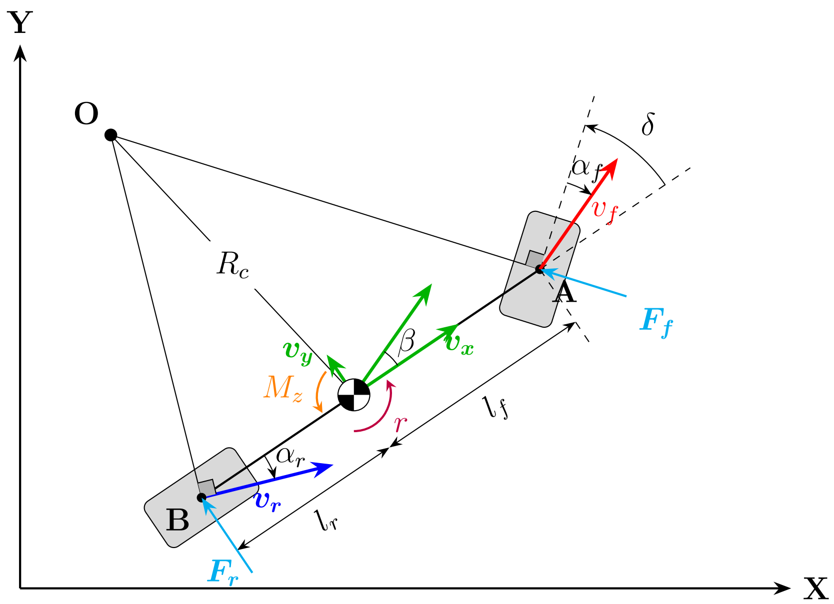

Figure 2.1: Linear Bicycle Model

2.1.1 Derivation of the Single Track Model

The lateral dynamics of the vehicle are derived using Newton's second law of motion for translation along the lateral y-axis and rotation about the vertical z-axis. The vehicle is assumed to be traveling at a constant longitudinal velocity v_x, the steering angles δ are assumed to be small and the model is assumed to move in a 2D-plane.

Because the vehicle's equations of motion are formulated in a body-fixed, rotating reference frame, the lateral acceleration a_y at the Center of Gravity (CoG) consists of two kinematic components. The first is the local rate of change of the lateral velocity ($\dot{v}_y$), and the second is the cross-coupling term ($v_x r$) which arises mathematically due to the rotation of the coordinate system itself at yaw rate r. This relationship is defined as:

$$a_y = \dot{v}_y + v_x r$$

Expressed in terms of the vehicle side slip angle β (where $v_y \approx v_x \beta$ for small angles), the lateral derivative becomes $\dot{v}_y \approx v_x \dot{\beta}$. Substituting this into the lateral equation of motion yields:

$$ma_y = mv_x(\dot{\beta} + r) = F_{yf} + F_{yr} \tag{2.1}$$

where m is the vehicle mass and F_{yf} and F_{yr} are the lateral tire forces generated at the front and rear axles, respectively.

$$F_{yf} = F_f \cos\delta \approx F_f$$
$$F_{yr} = F_r$$

The rotational equation of motion around the vertical z-axis is driven by the moment created by the lateral tire forces around the CoG:

$$M_z = I_z \dot{r} = l_f F_{yf} - l_r F_{yr} \tag{2.2}$$

where I_z is the vehicle's yaw moment of inertia and l_f and l_r are the distances from the CoG to the front and rear axles respectively, see Figure 2.1.

2.1.1.1 Linear Tire Forces and Slip Angles

Operating within the linear handling region, the lateral tire forces are modeled as being directly proportional to their respective tire slip angles (α_f and α_r):

$$F_{yf} = C_f \alpha_f \tag{2.3}$$

$$F_{yr} = C_r \alpha_r \tag{2.4}$$

where C_f and C_r represent the effective cornering stiffness of the front and rear wheels of the model respectively.

The tire slip angle is defined as the difference between the steering angle of the wheel and the angle of the velocity vector of the wheel. Using small angle approximations, the slip angles for the front and rear tires are kinematically derived as:

$$\alpha_f = \delta - \left(\frac{v_y + l_f r}{v_x} \right) \tag{2.5}$$

$$\alpha_r = 0 - \left(\frac{v_y - l_r r}{v_x} \right) \tag{2.6}$$

2.1.1.2 State Space Formulation

By substituting the slip angles in Equations 2.5 and 2.6 into the tire force Equations 2.3 and 2.4 and inserting these forces into the equations of motion 2.1 and 2.2, the system can be expanded and rearranged.

Isolating the state derivatives $\dot{\beta}$ and $\dot{r}$ yields the following system of differential equations:

$$\dot{\beta} = -\frac{C_f + C_r}{m v_x}\beta + \left(\frac{C_r l_r - C_f l_f}{m v_x^2} - 1 \right) r + \frac{C_f}{m v_x}\delta \tag{2.7}$$

$$\dot{r} = \frac{C_r l_r - C_f l_f}{I_z}\beta - \frac{C_f l_f^2 + C_r l_r^2}{I_z v_x} r + \frac{C_f l_f}{I_z}\delta \tag{2.8}$$

These linear ordinary differential equations are expressed in continuous state space form:

$$\dot{x} = Ax + Bu \tag{2.9}$$

where the state vector is defined as $x = [\beta, r]^T$ and the control input is $u = \delta$. The resulting system is given by:

$$\begin{bmatrix} \dot{\beta} \\ \dot{r} \end{bmatrix} = \underbrace{\begin{bmatrix} -\frac{C_f+C_r}{mv_x} & \frac{C_r l_r - C_f l_f}{mv_x^2} - 1 \\ \frac{C_r l_r - C_f l_f}{I_z} & -\frac{l_f^2 C_f + l_r^2 C_r}{I_z v_x} \end{bmatrix}}_{A} \begin{bmatrix} \beta \\ r \end{bmatrix} + \underbrace{\begin{bmatrix} \frac{C_f}{mv_x} \\ \frac{l_f C_f}{I_z} \end{bmatrix}}_{B} \delta \tag{2.10}$$

This state space representation completely describes the linear lateral and yaw dynamics of the vehicle, serving as both the foundation for system identification and the internal plant model for the optimal control algorithm.

2.2 System Identification

The unknown parameters of the bicycle model were estimated with help of system identification [3]. This section details the physical testing, data processing, and parameter estimation procedures, which were conducted using relevant international organization for standardization (ISO) standards as guidelines [4],[5].

2.2.1 Steady State Identification

The steady-state behavior of the vehicle is critical because it forms the basis of the ideal reference model used by the active controller. Consider the steady state where the vehicle travels at a constant longitudinal velocity v_x with a constant steering angle δ, meaning the transient state derivatives become zero ($\dot{\beta} = 0$ and $\dot{r} = 0$).

By setting the left side of the state space equation (Eq. 2.10) to zero and solving for the yaw rate r, the steady state yaw rate response was extracted:

$$r = \frac{v_x}{L + K_{us} v_x^2} \delta \tag{2.11}$$

where L is the vehicle wheelbase ($L = l_f + l_r$) and K_{us} represents the *understeer gradient*, an important vehicle dynamics metric that defines the vehicle's steady state handling characteristics [2]. The theoretical understeer gradient was calculated as:

$$K_{us} = \frac{m}{L} \left(\frac{l_r}{C_f} - \frac{l_f}{C_r} \right) \tag{2.12}$$

Theoretical frameworks, such as the ISO 4138:2021 standard, define the steady state circular driving conditions required to extract the understeer gradient K_{us} [4]. During a steady state turn, the slip angle β is small which means the kinematic radius of the vehicle trajectory can be approximated to:

$$R_c = \frac{v_x}{r} \tag{2.13}$$

By evaluating the steady state reference (eq. 2.11) response with respect to lateral acceleration (a_y), the understeer gradient was expressed as the derivative:

$$K_{us} = \frac{\partial(\delta - \frac{L}{R_c})}{\partial a_y} \tag{2.14}$$

The standard outlines the method to find the steady state equilibrium conditions of speed, steering wheel angle and turning radius by holding one of these parameters constant while varying the second and measuring the third. There are three different tests which all yield the same results but they mainly differ in testing space and the equipment available to the test taker. Each of these tests have small variations on how the varied variable will be changed.

The constant steering angle method was selected to determine the understeer gradient, where the steering wheel is held at a fixed angle and vehicle speed is progressively increased and the dynamic radius is calculated using Equation 2.13. However since the SbW system adjust the steering ratio based on speed, the steering angle of the rack is directly observed from the CAN bus and used for estimation of the understeer gradient.
This method was chosen over the ISO-defined constant radius and constant speed methods for two primary reasons: test space constraints and data fidelity.

First, the constant radius method was excluded due to the operational constraints of the testing area, which lack the painted visual markers required for the driver to accurately track a fixed circle. Second, the constant speed method (varying steering angle) was excluded to minimize driver induced measurement noise. Executing a perfectly smooth, continuous increase of the steering wheel while simultaneously holding constant speed is highly susceptible to human error. Such coupled inputs frequently result in high-frequency steering corrections that corrupt the lateral data. By utilizing the constant steering angle method, the driver physically anchors the steering wheel, thereby isolating the lateral input and yielding a significantly cleaner dataset for the subsequent linear regression analysis.

The test was conducted with the variation of continuous speed increase. Also general parameters are taken before the test begins such as the wind speed, temperature and tire type (winter tires), brand and pressure. Furthermore the car tires was warmed up by driving laps on the test track. In accordance to the standard, the test is taken in both directions with three repetitions, driving in one direction followed by driving in the other direction and then stopping for few minutes.

The test started with predetermining a fixed steering angle δ_{driver} to achieve a low speed radius, once determined the speed was slowly increased while holding a fixed steering angle and data was gathered for the lateral acceleration a_y, road wheel angle δ, yaw rate r and speed v_x. The speed steadily increased until a lateral acceleration larger than 5 m/s^2 was achieved while keeping the acceleration rate of increase below $0.1 m/s^2/s$.

The data was analyzed to calculate the understeer gradient in accordance with equation 2.14. In practice, linear regression was applied to the data to estimate the gradient. The theoretical accuracy of this linear approximation was validated using the **coefficient of determination** (R^2):

$$R^2 = 1 - \frac{\sum_i (y_i - f_i)^2}{\sum_i (y_i - \overline{y})^2} \tag{2.15}$$

where f_i is the predicted value from the linear regression model, y_i is the actual measurement and $\overline{y}$ is the mean value. A value closer to 1 indicates a better linear model fit [6].

2.2.2 Transient Response Identification

While the steady-state model acts as the target reference, the full dynamic transient model is needed to simulate the vehicle and ensure the controller remains stable before deployment on a real car. To make the dynamic model accurate, the unknown parameters yaw moment of inertia (I_z) and the effective cornering stiffnesses (C_f and C_r) must be estimated.

Grey-box modeling [3] is used here to estimate internal parameters of the given vehicle model from experimental data.
To estimate the cornering stiffness, the understeer gradient K_{us} was used as metric to determine the relation between the cornering stiffness for the back tires C_r and the front tires C_f. By rearranging Equation 2.12, the mathematical relationship between the front and rear cornering stiffness can be defined as:

$$C_r = \frac{l_f}{(\frac{l_r}{C_f} - K_{us}\frac{L}{m})} \tag{2.16}$$

ISO 7401:2011 explains the test methods used to evaluate the transient lateral response of vehicles [5]. The standard also provides specific criteria for determining the validity of the measured data and provides guidelines for how the data should be analyzed.

For this study, the random steering input maneuver was executed. The objective of this test is to continuously excite the vehicle's lateral dynamics across a broad frequency band (0.2 to 2.0 Hz). This method was chosen over the other ISO-defined transient tests such as the step-steer, pulse and swept-sine maneuvers for three primary reasons:
Firstly, it provides a highly rich, broadband dataset that is perfectly suited for frequency-domain system identification and spectral analysis (Welch's method). Secondly, it offers greater practical flexibility and is more robust against driver error compared to the swept-sine test, that requires the driver to perfectly execute continuously increasing frequencies over a long duration. Finally, the random input test is advantageous from a safety and facility constraint perspective. Because the steering inputs alternate rapidly, the vehicle's lateral deviation from the center line remains relatively small. This allows the test to be safely conducted on narrower test tracks, avoiding the need for the massive spatial footprint required by aggressive,

high-speed step or pulse maneuvers.

The test procedure was executed as follows:

- Wind speed, weather temperature, tire pressure and weight of car were noted and the car tires was warmed up by driving laps on the test track.
- The vehicle was driven at a constant longitudinal speed ($v_x = 80$ km/h) on the test track.
- The driver applied continuous, random steering wheel inputs of varying rates and amplitudes to excite the vehicle dynamics across a broad frequency spectrum.
- The amplitude of the steering input was carefully modulated to keep the vehicle strictly within its linear handling region of $a_y < 5m/s^2$.

To ensure statistical robustness and to capture slightly different operating points, a total of 17 individual test runs were recorded. During each run, the steering wheel angle, actual road wheel angle, vehicle speed, lateral acceleration and yaw rate were logged over the CAN bus. While the physical steering inputs generated a wide frequency response, the recorded data was truncated during signal processing. Only the frequency response within the 0.2 to 2.0 Hz range was utilized for the system identification.

In accordance with the standard, the spectral density $\hat{\Phi}_\delta(\omega)$ of the road wheel angle was estimated using Welch's method to analyze the frequency content of the driver's input [3]. In this approach, the time-domain data was divided into N overlapping segments, each of length M. To mitigate spectral leakage, a Hann window was applied to each segment before forming individual periodograms. The final spectral density estimate was then obtained by averaging these modified periodograms:

$$\hat{\Phi}_\delta(\omega) = \frac{1}{N}\sum_{i=1}^{N} \hat{\hat{\Phi}}_M^{(i)}(\omega) \tag{2.17}$$

The standard also outlines criteria to validate the data. The first criterion is that the spectral density must not vary by more than 12 dB within the 0.2 to 2.0 Hz frequency range. This ensures that the vehicle is adequately and evenly excited across the entire frequency band of interest.

$$10\log_{10}\left(\frac{\max(\Phi_\delta(\omega))}{\min(\Phi_\delta(\omega))}\right) \leq 12 \text{ dB} \quad \text{for } f \in [0.2, 2.0] \text{ Hz} \tag{2.18}$$

The second criterion is the magnitude-squared coherence function γ^2, a metric used to quantify the linear correlation between the vehicle output signal and the input signal [7]. The coherence function is bounded between 0 and 1. The closer the value to 1 the more correlation between the input and output signals, and the less the noise affect the output signal, meaning the mathematical transfer function at that frequency is highly reliable. The coherence function is defined as squared magnitude of the cross-power spectral density between the steering wheel angle and vehicle yaw rate $\hat{\Phi}_{r,\delta}$ divided by the product of their individual auto-power spectral densities $\hat{\Phi}_\delta$ and $\hat{\Phi}_r$:

$$\gamma^2 = \frac{|\hat{\Phi}_{r,\delta}(\omega)|^2}{\hat{\Phi}_{\delta}(\omega)\hat{\Phi}_{r}(\omega)} > 0.95 \quad \text{for } f \in [0.2, 2.0] \text{ Hz} \tag{2.19}$$

ISO 7401 dictates that for a transient test to be deemed acceptable, the coherence between the yaw velocity and the steering wheel angle must remain above 0.95 within the 0.2 to 2.0 Hz frequency range.

2.2.2.1 Grey-Box Parameter Estimation

The validated datasets were aggregated to form the official estimation dataset. To estimate the unknown parameters, MATLAB's System Identification Toolbox was employed [8].

First, the vehicle's mass (m) and wheelbase dimensions (l_f, l_r), were set as fixed parameters. The equation 2.16 was used as a strict mathematical constraint to link C_f and C_r.

Using the `idgrey` function, the continuous state space structure of the linear single track model was constructed. Finally, the `greyest` algorithm was executed using the estimation dataset. The numerical search iteratively adjusted the single free parameter (C_f and I_z) to minimize the error between the measured vehicle response and the simulated model response for both yaw rate and lateral acceleration. Including lateral acceleration alongside yaw rate is critical for robust parameter identifiability. While yaw rate captures the rotational moments acting on the vehicle, lateral acceleration provides a direct measurement of the total lateral forces. Utilizing both physical states overconstrains the optimizer, preventing the solver from converging on mathematically valid but physically unrealistic combinations of cornering stiffnesses. Furthermore, this multi-variable approach mitigates the influence of individual sensor noise and ensures the unmeasured lateral velocity state remains physically bounded during the transient simulation.

2.3 Model Validation

Before the model with its estimated parameters can be trusted to tune the control system, its accuracy must be proven. This section details the validation procedure used to ensure that the estimated parameters and model represent the true physical vehicle's dynamics, rather than just overfitting to the specific maneuvers used during estimation.

2.3.1 Overfitting and the Holdout Method

According to system identification theory, an optimization algorithm will naturally minimize the error on the specific data used to estimate its parameters [9]. However evaluating a model solely on this estimation data may result in overfitting, where the model begins to capture the specific noise realizations and unmodeled disturbances of those exact test runs rather than the underlying physical dynamics of the vehicle. To mitigate this risk, a holdout validation strategy was employed. A completely independent validation dataset was collected by driving the vehicle for two continuous laps on the test track. During this sequence, a variety of dynamic manoeuvrers were performed, including lane changes and random transient steering inputs. This ensured that the model was evaluated across diverse driving conditions entirely separate from the maneuvers used during parameter estimation.

2.3.2 Evaluation Metrics (NRMSE)

The validation dataset was then analyzed to evaluate the model's performance. The simulated vehicle response was generated using the measured longitudinal velocity (v_x) and steering angle (δ) as inputs. The response was then compared against the actual yaw rate.
To mathematically quantify this accuracy, the Normalized Root Mean Square Error (NRMSE) was utilized. As established in MATLAB's System Identification Toolbox [8], the NRMSE provides a consistent evaluation across different maneuvers by dynamically normalizing the prediction error against the signals overall variance.
To express the accuracy as an intuitive percentage, the final NRMSE model fit is formulated as:

$$\text{Fit } (\%) = 100 \cdot \left(1 - \frac{||y - \hat{y}||_2}{||y - \bar{y}||_2}\right) \tag{2.20}$$

where y is the vector of the measured states, $\hat{y}$ is the vector of the simulated states and $\bar{y}$ is the mean value of the measured data. The notation $||\cdot||_2$ denotes the Euclidean (L_2) norm.
In addition to this numerical metric, time-domain plots were generated to visually illustrate the correlation between the measured and predicted yaw rate and lateral acceleration.

2.3.3 Frequency Response Validation

The empirical transfer function $G_{r,\delta}(\omega)$ for the dynamic relation between the road wheel steering input and the vehicle response was calculated by dividing the cross-power spectral density of the output and input ($\Phi_{r,\delta}(\omega)$) by the auto-power spectral density of the steering input $\Phi_\delta(\omega)$ [3]:

$$G_{r,\delta}(\omega) = \frac{\hat{\Phi}_{r,\delta}(\omega)}{\hat{\Phi}_\delta(\omega)} \tag{2.21}$$

This empirical transfer function encapsulates the true physical transient dynamics of the vehicle. It served as the baseline against which the theoretical transfer function of the bicycle model was validated once the unknown tire parameters were estimated.

2.4 Control Architecture and Algorithm Design

With the vehicle's lateral dynamics mathematically modeled and validated, this section details the software implementation. It explains how the steady-state model is used as a reference target and how the dynamic model is used to tune and guarantee the stability of the active closed-loop controller before physical deployment.

The primary objective of the active disturbance attenuation system is to minimize the tracking error between the reference yaw rate (r_{ref}) and the actual vehicle yaw rate (r) measured by the Inertial Measurement Unit (IMU).
The development of the control system followed a structured, model-based (MB) methodology. The process was divided into four sequential phases, which dictate the structure of the subsequent sections:

1. **Architecture Selection in Simulation:** Analytical evaluation of classical (PID) and optimal (LQR) control strategies to determine the most suitable architecture.
2. **Tuning and Stability Analysis:** Establishing baseline controller gains and mathematically proving system robustness using frequency-domain analysis (Bode and Nyquist) on the simulated plant.
3. **Prototype vehicle Calibration:** Deploying the theoretical controller to the physical prototype vehicle to validate stability limits and fine-tune the final feedback gain.
4. **Full-Scale Dynamic Testing:** Evaluating the final closed-loop system through dynamic maneuvers and external disturbance scenarios.

2.4.1 Controller Implementation and Hardware Constraints

The controllers were developed and tuned in simulation, and could later be deployed as a simulated Electronic Control Unit (ECU) using Vector CANoe and communicate with the physical SbW vehicle. The control logic operates in a cyclic task with a discrete time step of $\Delta t = 5$ ms (200 Hz), reading vehicle data and writing the corrective overlay requests directly over the CAN bus.

The total steering angle applied to the road wheels (δ) is defined as the sum of a feedforward command and the controller's feedback correction:

$$\delta = \delta_{driver} + \delta_{add} \tag{2.22}$$

The human driver acts as the primary feedforward controller by providing the steering angle (δ_{driver}), while the active closed-loop system provides the corrective feedback overlay (δ_{add}) to stabilize the vehicle against transient errors and external disturbances.

A practical limitation in the system was the resolution of the CAN bus communication. The steering overlay signal (δ_{add}) that the controller sends to the vehicle was restricted to an 8-bit signed integer. To translate the continuous output from the controller into a valid CAN message, the calculated steering command was scaled by the predefined signal resolution factor of $\frac{1}{1024}$ rad/bit and rounded to the nearest integer. To prevent overflow, the integer was then explicitly saturated within the software to remain strictly between -128 and $+127$. This resulted in the physical steering overlay being applied in discrete steps, where each step corresponds to 0.056°.

2.4.2 Steady State Cornering and Reference Model

To enable closed-loop control, an ideal target vehicle motion is defined. This ideal target was in this project represented by the steady state reference yaw rate (r_{ref}, Eq. 2.11) of the linear single track model, which describes how the vehicle behaves under ideal, undisturbed conditions for a given steering input and velocity.

In the physical prototype vehicle, the measured road wheel angle (δ) available on the CAN bus is the sum of the driver-commanded wheel angle (δ_{driver}) and the active overlay angle generated by the controller (δ_{add}). To calculate the correct steady-state reference yaw rate and find the yaw rate error, the driver's true input needed to be mathematically isolated:

$$\delta_{driver} = \delta - \delta_{add} \tag{2.23}$$

Assuming a general proportional feedback structure where $\delta_{add} = K_{fb}(r_{ref} - r)$, with K_{fb} representing a generic feedback gain. Substituting this relationship into the steady state reference equation ($r_{ref} = G_{ss} \cdot \delta_{driver}$):

$$r_{ref} = G_{ss} \cdot (\delta - K_{fb}(r_{ref} - r)) \tag{2.24}$$

where G_{ss} is the theoretical steady state gain derived from the linear bicycle model, defined as:

$$G_{ss} = \frac{v_x}{L + K_{us} v_x^2} \tag{2.25}$$

By expanding and rearranging the equation to solve for r_{ref}, the reference formula implemented in the software is derived:

$$r_{ref} = \frac{G_{ss}(\delta + K_{fb} r)}{1 + G_{ss} K_{fb}} \tag{2.26}$$

This ensures that the calculated target yaw rate accurately reflects the human drivers input. Allowing it to be utilized by any underlying feedback control strategy.

2.4.3 Proportional-Integral-Derivative (PID) Control

In vehicle dynamics, PID-based controllers are frequently utilized as the preferred starting point for lateral control due to their model free approach, simplicity in tuning and robustness against parameter uncertainties [10]. Therefore the PID controller was chosen as the baseline strategy and starting point.

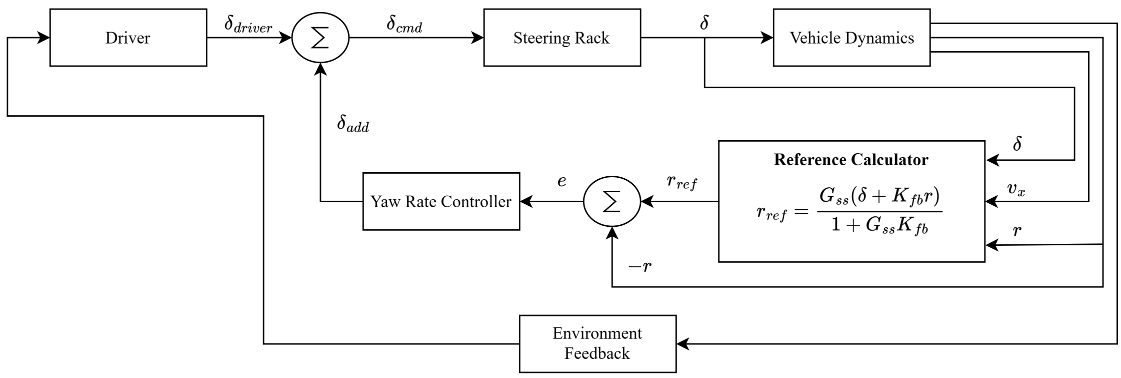

Figure 2.2: Block Scheme of the control system

A full PID structure was initially implemented and evaluated within the MATLAB/Simulink simulation environment to assess the individual contribution of each control term. Based on the simulation outcomes (see Section 3.3.2), the integral component was discarded first. This decision was driven by observed integrator windup during transient maneuvers and the theoretical redundancy of integral action given the human-in-the-loop dynamics. Subsequently, the pure P and PD controllers were compared. Since the simulations revealed only marginal performance differences between the P and PD controllers, the derivative term was also excluded. Ultimately, the pure P-controller was selected for the implementation in the prototype vehicle.

2.4.4 Linear Quadratic Regulator (LQR)

A Linear Quadratic Regulator was evaluated in simulation to determine whether optimal multi-state feedback offered any advantages over the proportional controller. The LQR computes an optimal gain matrix $K = [K_1, K_2]$ that minimizes a quadratic cost function trading off state error against control effort, using the state-space matrices A and B derived from the grey-box estimation.

A constraint of this application is that the sideslip angle β could not be directly measured on the vehicle. While β can theoretically be estimated by integrating lateral acceleration, this approach accumulates drift over time and is unreliable for real-time control. The LQR was therefore evaluated in simulation only, to assess whether penalizing both states simultaneously through a single control input produced a meaningful performance advantage.
Because the controller operated as a discrete 5 ms task, the continuous vehicle model was converted to discrete time using a zero-order hold (ZOH) method. A 50 ms transport delay was incorporated before computing the discrete LQR gains to reflect the physical hardware constraints. The state weighting matrix Q and control effort weight R were varied systematically to evaluate the trade-off between yaw rate tracking and sideslip regulation, as presented in Section 3.3.3.

2.4.5 Stability Analysis

To estimate the stability and robustness of the controller several methods were utilized. Methods that evaluated the effectiveness of the controller and a comparison between open-loop and closed-loop systems. The system plant will be denoted as $G(s)$ while the controller will be $G_c(s)$. A continuous time delay was also introduced to the system as e^{-sT_d}. The open loop transfer function $L(s)$ can be formulated as:

$$L(s) = G_c(s)G(s)e^{-sT_d} \tag{2.27}$$

The most fundamental criterion to determine the stability of the system is the location of the poles for the transfer function $G(s)$. A system is strictly stable if all its poles are located in the left half plane of the real-imaginary axis.

Root Locus is a graphical plot used to determine how these closed-loop poles will shift as a specific parameter is varied from zero to infinity. In this thesis, Root Locus analysis was explicitly employed to evaluate the theoretical stability boundaries of the model-free controller. By observing how increasing the proportional gain pulled the poles toward the unstable right half-plane, an appropriate and safe initial proportional gain (K_p) could be determined prior to conducting the time-domain simulations.

2.4.5.1 Frequency response

To ensure the tuned controllers remained robust despite the hardware delay, frequency response analysis is utilized. The Bode plot was employed to analyze how the open-loop system reacted across different frequencies, allowing for the extraction of key margins that guarantee closed-loop stability:

- **Gain Crossover Frequency (ω_{gc}):** The frequency at which the Amplitude Ratio (AR) of the open-loop system is $AR_{OL}(\omega_{gc}) = 1$ (or 0 dB).
- **Phase Crossover Frequency (ω_{pc}):** The frequency at which the phase angle of the open-loop system crosses the instability threshold, $\varphi_{OL}(\omega_{pc}) = -180°$.
- **Gain Margin (GM):** A measure of robustness that shows how much the controller gain can be multiplied before the open-loop magnitude reaches 0 dB at the phase crossover frequency.
- **Phase Margin (PM):** A measure of robustness that shows how much additional phase delay can be introduced to the system before the phase reaches $-180°$ at the gain crossover frequency.

The Bode Stability Criterion which explicitly accounts for systems with time delays was used to analyze the controller stability. The criterion defines a closed-loop system as stable if:

$$AR_{OL}(\omega_{pc}) < 1 \tag{2.28}$$

Because time delays introduce phase lag into the system. To ensure the chosen tuning parameters were safe, the maximum physical time delay (t_{max}) that the system could tolerate was calculated directly from the achieved Phase Margin (where

$PM = 180° + \varphi_{OL}(\omega_{gc})$):

$$t_{max} = \frac{PM}{\omega_{gc}} \cdot \frac{\pi}{180} \tag{2.29}$$

2.4.5.2 System Robustness

The Nyquist stability criterion was also utilized during tuning to determine the absolute stability of the delayed system. The criterion states that a system is stable if:

$$Z = N + P = 0 \tag{2.30}$$

where N is the number of times the Nyquist plot encircles the $(-1, 0j)$ point in the clockwise direction and P is the number of open-loop poles in the right half-plane.

While frequency domain analysis tools like Bode and Nyquist plots can handle a time delay in its exponential form e^{-sT_d}, other algebraic root finding methods cannot. Therefore the Padé approximation is introduced to transform the pure time delay into a rational transfer function:

$$P_M^N(s) = \frac{\sum_{n=0}^{N} a_n s^n}{\sum_{m=0}^{M} b_m s^m} \tag{2.31}$$

The coefficients a_n and b_m are chosen such that the Taylor expansion of the original exponential delay with the same order is equal to the Padé approximation [11].

Finally, the robustness of the tuned controller against external disturbances was evaluated using the Sensitivity function, $S(s)$:

$$S = \frac{1}{1 + L(s)} \tag{2.32}$$

The maximum amplitude ratio (peak gain) of the Sensitivity function over all frequencies is denoted as M_s:

$$M_s = \max_{\omega} |S(j\omega)| \tag{2.33}$$

M_s is the inverse of the shortest distance from the open-loop transfer function curve to the critical instability point $(-1, 0j)$ in the Nyquist plot. A lower value of M_s confirms a higher overall stability margin. The controller was tuned to ensure that the value M_s was within the recommended robust range of 1.2 to 2.0 [12].

2.4.6 Fine-Tuning in the Vehicle

The theoretical stability margins and initial controller gains were established using the linear single-track model in MATLAB. However, to confirm the robustness it required empirical validation in the actual SbW vehicle.

The controller was deployed to the prototype vehicle via the CANoe environment. An empirical stability analysis was conducted by systematically increasing the proportional gain (K_p). By deliberately pushing the gain toward the theoretical instability threshold identified by the Root Locus and Nyquist analyses, overlay steering oscillations could be observed (see Figure 3.17).

Once the true physical instability limit was found on the test track, the gain was lowered to regain a robust stability margin. The objective of this final calibration phase was to bridge the gap between theoretical robustness and physical reality, ensuring an optimal balance between aggressive disturbance attenuation and a smooth, predictable steering feel for the human driver.

2.5 Vehicle Testing

While analysis in simulation provides theoretical guarantees of stability, the ultimate proof of the controller's safety and efficacy must be demonstrated in reality. This section outlines the dynamic maneuvers designed to provoke the vehicle and evaluate the controller's ability to attenuate real external disturbances.

Before every testing session, the vehicle's total mass and weight distributions were measured on a vehicle scale. To isolate the lateral dynamics, all maneuvers were executed at a constant longitudinal velocity maintained by the vehicle's cruise control system.

The physical maneuvers were initially performed in an unassisted configuration to establish a dynamic baseline. Thereafter, the active controller was engaged and the maneuvers were repeated on the same track. During all runs, vehicle data including the steering angle, vehicle speed, actual yaw rate, lateral acceleration and the applied corrective overlay (δ_{add}), were continuously logged via the vehicle's CAN bus for analysis. The primary objective of these maneuvers was to introduce sudden changes in yaw rate, forcing the controller to compensate and allowing for a performance analysis.

2.5.1 Lane Change Maneuvers

To evaluate the controller's transient response and its ability to handle sudden, aggressive inputs, lane change maneuvers were performed. The maneuver requires rapid changes on the steering wheel that induce significant overswing and large instant spikes in the vehicle yaw rate. By generating a substantial tracking error at first input and with the overswing it evaluates the controllers responsiveness and damping capability.

During the practical execution of the lane change maneuver, the velocity (V_x) was held constant. The driver initiated the maneuver by applying a rapid steering wheel angle (δ_{driver}) of approximately 140° to one side. This initial input was immediately followed by an aggressive counter steer to the opposite direction. Finally, the steering wheel was rapidly returned to neutral position ($\delta_{driver} = 0°$). The maneuver was performed several times for both closed and open loop to have sufficient logs and rule out driver inconsistencies.

2.5.2 Disturbance attenuation Tests Using a Trailer

To specifically test how well the active lateral stabilization system handles external disturbances, disturbance attenuation tests were conducted with a trailer attached to the car. Towing a trailer inherently reduces the stability margin of the combination vehicle and acts as an external lateral force on the rear axle.

The trailer was tested using two different loading configurations to capture varying real world driving scenarios. The first configuration (Configuration 1) utilized a standard load with a positive tow-hook pressure. The second configuration (Configuration 2) utilized a very rear biased load, yielding a negative tow-hook pressure. This loading distribution has the trailers CoG behind its axle. This was chosen to deliberately introduce instability and continuous trailer sway.

The vehicle combinations was driven at a constant speed of 80 km/h. To trigger the disturbance attenuation logic, the driver introduced random excitations by doing random steering input across a broad frequency span. The logged data was then analyzed to verify if the controller could automatically detect and damp the resulting yaw oscillations caused by the trailer.

2.5.3 Subjective Evaluation

While quantitative metrics such as RMS error and phase delay provide objective proof of the controller performance, they do not fully capture the human drivers perception of the system. Because the SbW controller operates with a human-in-the-loop, a subjective evaluation is critical to ensure that the active steering interventions do not feel unnatural or disconnected for the driver.

A subjective analysis was performed with 12 participants to get feedback on the implementation and if there was any noticeable change. The maneuvers that were conducted was:

- Lane change
- Driving with trailer
- Lane Change on gravel surface

Experienced drivers will perform the different maneuvers however for the trailer driving normal passengers could partake and be a part of the evaluation. The gravel surface was selected to deliberately reduce the tire-road friction coefficient, thereby facilitating a larger vehicle side slip angle. During the gravel maneuver, the driver was instructed to accelerate to a steady-state velocity of approximately 60 km/h and subsequently perform a severe evasive lane change maneuver. This dynamic excitation was specifically designed to provoke a substantial transient yaw rate disturbance.

To evaluate the efficacy of the closed-loop control system during the gravel maneuver, the same vehicle states as the lane change were continuously logged via the vehicle's CAN bus. These signals was processed and used to calculate the RMS tracking error between the ideal reference yaw rate and measured yaw rate to illustrate the controller ability to help the driver stabilize the vehicle and to test the controller performance even when the linear assumptions of the reference model begin to degrade.

After the tests, the drivers were asked to fill in a form regarding the experience of the vehicle with and without the controller. The questionnaire utilized a scale to quantify the drivers subjective experience, including vehicle stability, steering effort, predictability of the vehicle trajectory and overall sense of safety.

The questionnaire can be found in the Appendix chapter A.1

3

Results

3.1 System Identification

The MB control strategy relies heavily on the accuracy mathematical model of the vehicle dynamics. This section presents the results from the steady-state and transient system-identification. These identified parameters were utilized to construct the plant model, which the closed-loop disturbance attenuation controller is evaluated.

3.1.1 Steady-State Characteristics & Understeer Gradient

To determine the vehicle understeer gradient K_{us}, the steady-state circular test method detailed in Section 2.2.1 was executed using the prototype vehicle. The environmental conditions and vehicle specifications recorded prior to the test are summarized in Table 3.1.

Occupants	2 x 80 kg
Total Vehicle Mass (m)	2428 kg
Tire Type	Winter tires (7 mm tread depth)
Tire Brand	Continental, Viking Contact 8
Tire Size	255/45 R 19 104 T XL
Tire Pressure	275.8 kPa
Temperature	-9°C
Wind Speed	< 2 m/s

Table 3.1: General parameters for the prototype vehicle

The test maneuver was targeted at a fixed steering angle of $\delta_{driver} = 1.0 \pm 0.1$ rad. To ensure the vehicle's handling characteristics are symmetric and not biased by the test track or the vehicle's static weight distribution, the maneuver was executed in both directions, three repetitions for left-hand turns and three for right-hand turns.

Figure 3.1 illustrates the steering wheel angle and corresponding longitudinal vehicle speed for a single representative repetition (Dataset 3) in the prototype vehicle. Concurrently, Figure 3.2 validates that the maneuver remained strictly within the steady-state region. To accurately calculate the rate of lateral acceleration increase (jerk) without amplifying high-frequency sensor noise. A second-order polynomial was fitted to the lateral acceleration time-series.

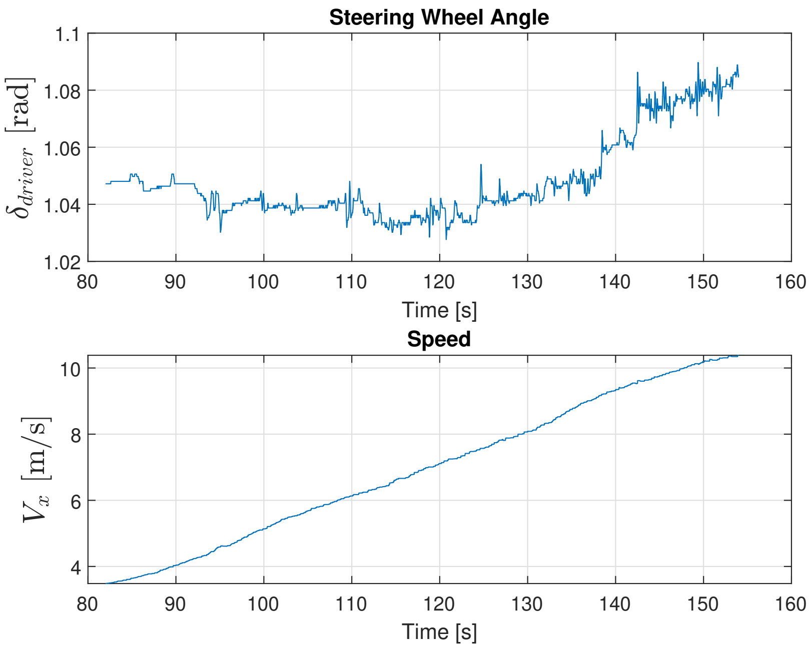

Figure 3.1: Steering wheel angle and speed for the prototype vehicle test run 3

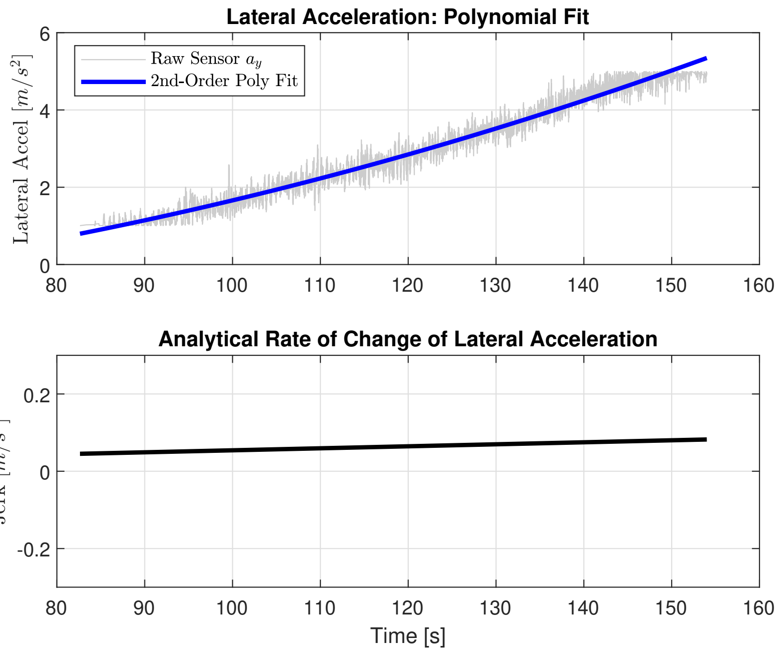

Figure 3.2: Lateral acceleration and jerk for the prototype vehicle test run 3

While the figures confirm the successful execution of an individual maneuver, to verify the integrity of all datasets prior to parameter extraction. Table 3.2 summarizes the extreme values for all six recorded test repetitions. Across all runs, the maximum jerk never exceeded the 0.2 m/s^3 limit and the steering wheel angle variations remained sufficiently bounded.

Table 3.2: Summary of validation metrics across all test repetitions

Test Repetition	Max Jerk$[m/s^2]$	Min $\delta_{driver}[rad]$	Max $\delta_{driver}[rad]$
1	0.095	1.026	1.103
2	0.073	0.936	1.056
3	0.082	1.028	1.090
4	0.073	0.976	1.075
5	0.064	0.963	1.101
6	0.165	1.016	1.089

Having confirmed that all six repetitions strictly satisfy the steady-state kinematic criteria, the data segments corresponding to the linear handling region (lateral accelerations between 1.0 m/s^2 and 5.0 m/s^2) were extracted for analysis.
In accordance with Equation 2.14, a steady-state handling diagram is constructed by plotting the kinematic adjusted steering angle ($\delta - \frac{L}{R_c}$) against the measured lateral acceleration (a_y). Figure 3.3 illustrates this relationship for a single test repetition run in prototype vehicle (Dataset 3).

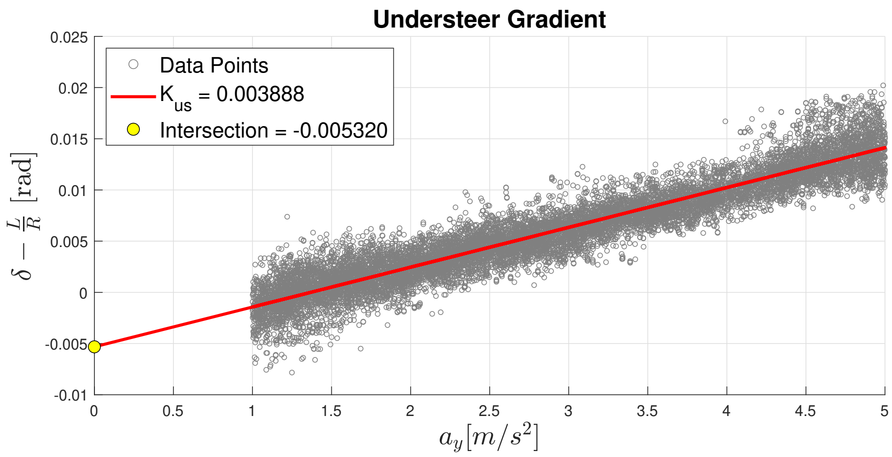

Figure 3.3: Steady-state handling diagram for test repetition 3

As established in Section 2.2.1 the understeer gradient is defined as the slope of this curve within the linear regime. A linear regression model was fitted to these extracted data points. The slope of this regression line yields the exact understeer gradient for that specific test repetition, while the coefficient of determination (R^2) evaluates the statistical fidelity of the linear approximation.

To ensure statistical reliability, this linear regression analysis was applied to all six test repetitions. Table 3.3 summarizes the extracted understeer gradient from all the measurments, the y-intercept (which theoretically approaches zero) and the R^2 value for each individual dataset.

Table 3.3: Linear regression results for all steady-state test measurements

Test Repetition	Understeer Gradient, K_{us} (rad/(m/s^2))	y-intercept (rad)	R^2
1 (Left)	4.00×10^{-3}	-5.52×10^{-3}	0.88
2 (Left)	4.05×10^{-3}	-5.49×10^{-3}	0.88
3 (Left)	3.89×10^{-3}	-5.32×10^{-3}	0.89
4 (Right)	3.51×10^{-3}	-1.67×10^{-3}	0.84
5 (Right)	3.48×10^{-3}	-1.62×10^{-3}	0.86
6 (Right)	3.70×10^{-3}	-2.53×10^{-3}	0.86

The data demonstrates high repeatability across all test runs. It should be noted that high-frequency noise from the IMU sensor, the inherent mathematical simplifications of the single-track model and physical road surface irregularities (such as bumps and uneven camber) introduced unmodeled dynamic excitations that prevented the R^2 metric from reaching higher theoretical values. However, as illustrated in Figure 3.3, the vehicle clearly exhibits linear behavior, definitively validating the use of the linear bicycle model assumptions within this operational envelope.

To determine the definitive vehicle parameter, the calculated slopes from the six repetitions were averaged. The final calculated understeer gradient for the vehicle equipped with winter tires yielded a value of:

$$K_{us} = 0.00377 \text{ rad/(m/s}^2) \tag{3.1}$$

Because this gradient is strictly positive ($K_{us} > 0$), it physically confirms that the vehicle exhibits natural understeering characteristics. This empirically derived value physically characterizes the vehicle's steady-state cornering behaviour. Consequently, this parameter is now locked in and utilized as a strict mathematical constraint for identifying the transient tire cornering stiffnesses (C_f and C_r) in the subsequent grey-box estimation phase, as well as for calculating the steady-state yaw reference in the vehicle controllers.

3.1.2 Grey-Box Parameter Estimation (Transient Response)

To determine the transient response of the vehicle and to calculate the yaw moment of inertia and cornering stiffness, the random input method detailed in Section 2.2.2 was executed, while the static specifications for the prototype vehicle remained identical to those in Table 3.1, the environmental test conditions differed and are shown in Table 3.4.

Table 3.4: General parameters for prototype vehicle before executing the random input driving test

Temperature	4 °C
Wind speed	3-4 m/s

Before executing the frequency-domain spectral analysis, the time-domain execution of the maneuvers was verified to ensure compliance with the constraints established in Section 2.2.2. Figure 3.4 illustrate the speed and lateral acceleration measurements for dataset 3. As shown in the bottom subplot, the longitudinal speed (v_x) was successfully maintained at the target velocity of 80 km/h, with only minor fluctuations. In the top subplot the peak lateral acceleration (a_y) remained bounded below the 4.0 m/s^2 threshold. This result is consistent with all 17 datasets, confirming the vehicle operated purely within the linear handling region.

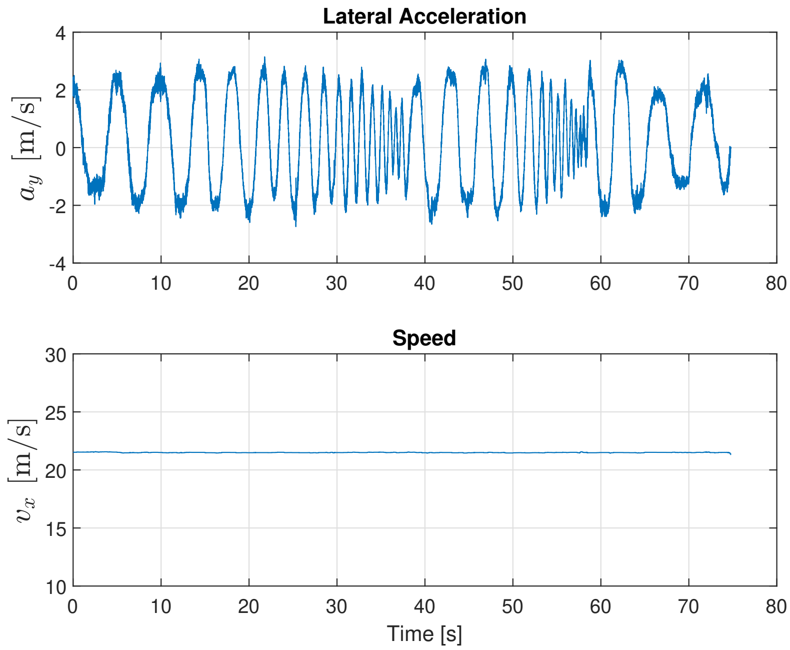

Figure 3.4: Lateral acceleration and speed measurements diagram for test Dataset 3

Prior to extracting the vehicle's dynamic transfer function, the spectral quality of the aggregated training data was evaluated using Welch's method, as detailed in Section 2.2.2.
The frequency content of the driver's steering input was validated to ensure adequate broadband excitation. Figure 3.5 illustrates the relative Power Spectral Density (PSD) of the road steering wheel angle ($\hat{\Phi}_\delta(\omega)$), normalized to the lowest frequency of interest (0.2 Hz).

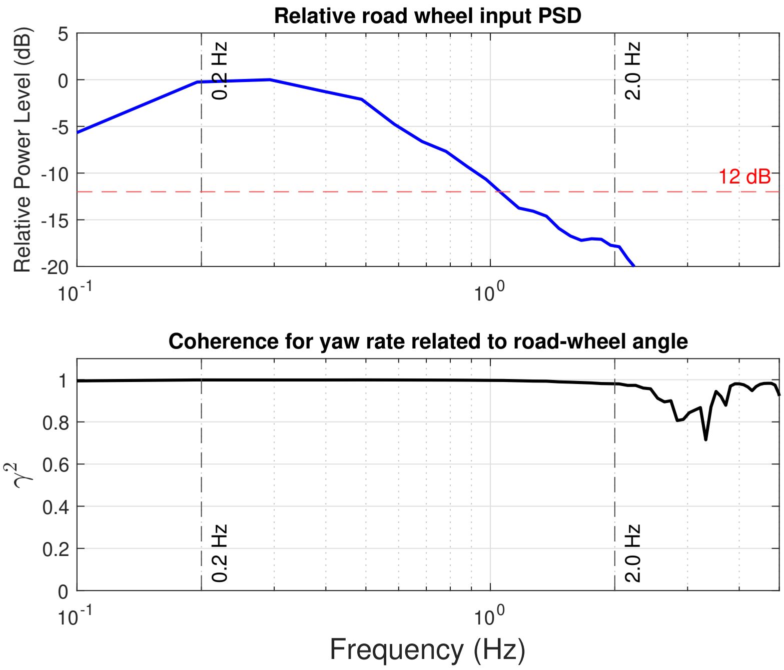

Figure 3.5: Relative Power Spectral Density of the steering wheel input measurements

Equation 2.18 dictates that the input spectral density should not experience a power drop of more than 12 dB within the 0.2 to 2.0 Hz frequency range. Upon evaluating the test data, the maximum variation of the steering wheel input PSD within this specified range was calculated to be 17.73 dB, exceeding the recommended limit. This deviation primarily occurred due to a drop in input power at higher frequencies (above 1.1 Hz), indicating that the driver did not physically generate sufficient high-frequency excitation during the manual maneuver. However, ISO 7401 permits the use of such data provided the extent of the ratio is recorded and the underlying data quality is otherwise verified via the coherence function.

As depicted in Figure 3.5, the coherence between the steering input and the yaw rate output ($\gamma^2_{r,\delta}$) remained exceptionally high, averaging approximately 0.993 across the entire 0.2 to 2.0 Hz band. This near-perfect correlation satisfies the ISO requirement of remaining above 0.95. It demonstrates an excellent signal-to-noise ratio and confirms a strictly linear relationship between the input and output. Therefore, the resulting frequency response estimates are deemed highly reliable for subsequent system identification.

The grey-box parameter estimation was then executed in accordance with Section 2.2.2.1. To maximize the data utilized by the prediction-error minimization algorithm (greyest), all measurements from the 17 datasets were merged into a single multi-experiment data object. The algorithm was initialized with a continuous-time state-space representation of the bicycle model. The optimization converged successfully on a final estimate for C_f and I_z. Consequently, C_r was analytically derived. The final dynamic parameters defining the vehicle model are illustrated in Table 3.5.

Table 3.5: Final derived and estimated vehicle parameters using winter tires.

Parameter	Symbol	Value
Yaw moment of inertia (Estimated)	I_z	$2877.18 \text{ kg} \cdot \text{m}^2$
Front cornering stiffness (Estimated)	C_f	132576.12 N/rad
Rear cornering stiffness (Calculated)	C_r	218234.75 N/rad

The time-domain fidelity of this parameterized model across the training datasets is summarized in Table 3.6, which details the NRMSE fit percentages for both lateral acceleration and yaw rate measurements.

Table 3.6: Model Fit Percentage For the Training data

Training Dataset	NRMSE Model Fit (%)	
	Lateral Accel (a_y)	Yaw Rate (r)
1	68.25	83.86
2	67.19	77.39
3	71.39	81.48
4	64.98	81.35
5	70.68	80.46
6	67.52	82.59
7	72.25	82.77
8	66.39	81.61
9	70.97	82.76
10	65.54	80.72
11	68.64	81.82
12	63.36	79.69
13	62.25	72.82
14	62.41	76.03
15	67.3	80.6
16	67.53	81.21
17	68.96	81.92

3.2 Model Validation

3.2.1 Independent Dataset Cross-Validation (NRMSE)

To verify that the estimated parameters and single track model generalize to unseen driving conditions without overfitting the training data, the model was evaluated against the independent holdout dataset as described in Section 2.3.1. The measured longitudinal velocity and steering angle from this sequence were fed into the mathematical model and the resulting simulated yaw rate was compared against the physical IMU sensor data.

The time-domain correlation between the physical vehicle and the mathematical simulation is illustrated in Figure 3.6.

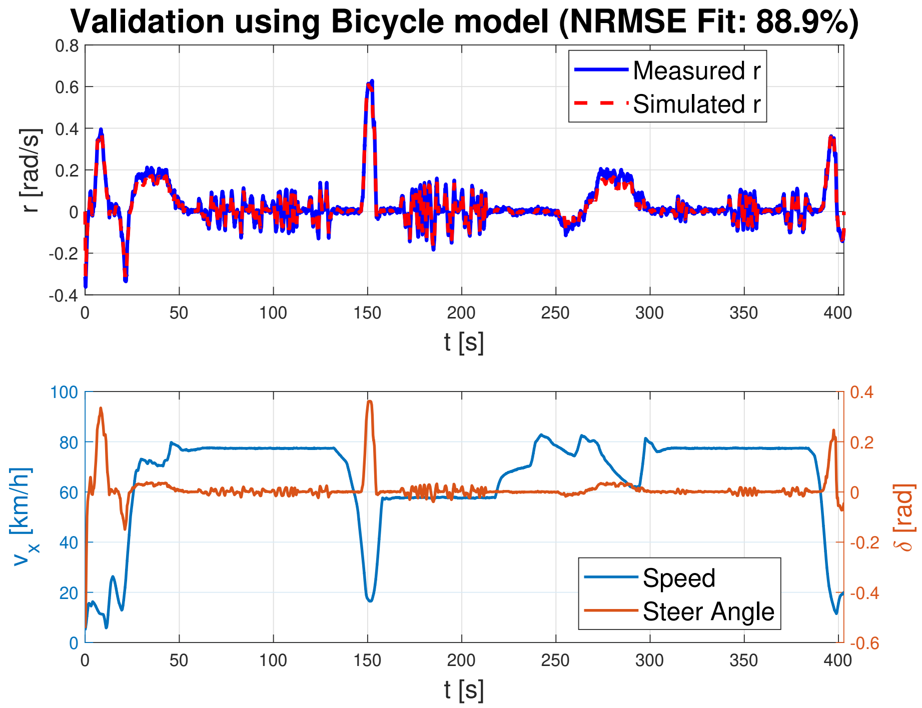

Figure 3.6: Time-domain validation showing the measured vehicle response, the simulated model response and the measured input signals on an independent track driving dataset.

Visual inspection of the plotted signals demonstrates that the simulated model closely tracks the actual vehicle yaw rate.
A quantifiable evaluation using NRMSE Equation 2.20 yielded a model fit of 88.9% for the yaw rate, showcasing a high degree of predictive correlation across the unseen track maneuver.

3.2.2 Frequency Domain Validation

To validate the fundamental dynamic fidelity of the model, its theoretical frequency response was compared against the empirical transfer function ($G_{r,\delta}$) derived from the 17 merged training datasets using Welch's spectral analysis.

Figure 3.7 shows that the theoretical model successfully captures the fundamental dynamic bandwidth and high-frequency roll-off of the vehicle's yaw response. A static magnitude offset is present at lower frequencies, indicating the physical vehicle exhibits a slightly higher steady-state yaw gain. This deviation is a accepted limitation of the linear 2-DOF bicycle model. Because the rear cornering stiffness (C_r) was strictly coupled to the front axle via the steady-state understeer gradient constraint (K_{us}), the model assumes a perfectly rigid planar chassis. In reality, dynamic steering maneuvers induce unmodeled three-dimensional kinematic compliances. However, despite this static DC-gain offset, the model accurately tracks the dynamic frequency

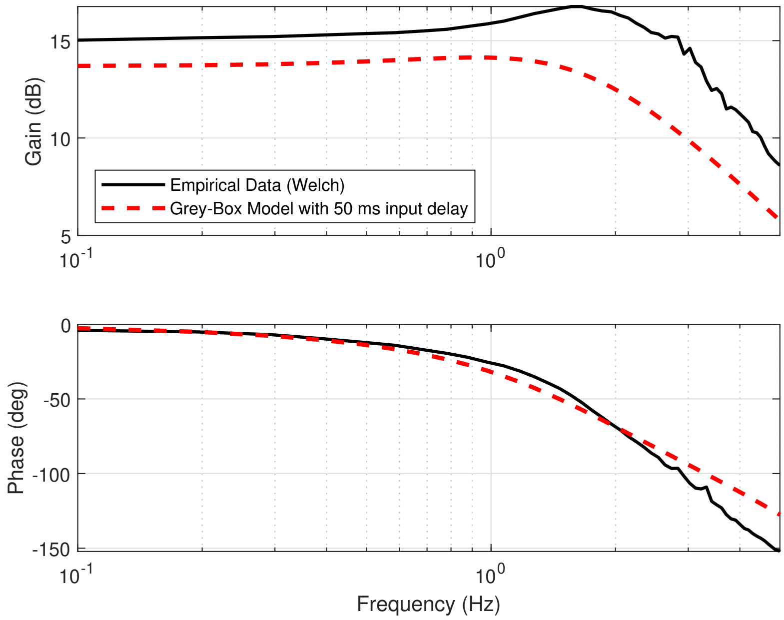

Figure 3.7: Frequency Domain Model Validation with input delay = 30 ms

roll-off, which is the primary objective of transient system identification.

Regarding the phase response, the single track model assumes instant tire force generation. To accurately reflect the physical transport lag of the chassis, a lumped equivalent delay of 30 ms was incorporated into the theoretical model. As shown in the Bode plot, this empirically tuned delay successfully anchors the theoretical phase to the steeper high-frequency roll-off of the physical vehicle.
Consequently, the validated mathematical model is deemed highly reliable as it successfully captures the fundamental lateral dynamics of the SbW prototype vehicle within the defined operating region ($a_y < 5$ m/s^2).

3.3 Controller Performance

This section presents the theoretical stability limits and the simulated time-domain tracking performance of the different controller variations, ultimately justifying the final architecture selected for physical SbW implementation.

3.3.1 Control Synthesis and Theoretical Stability

To determine the initial stability boundaries and evaluate the impact of hardware limitations, a Root Locus analysis was conducted for the proportional gain (K_p). The analysis compared an ideal, instantaneous system against a realistic system incorporating a 50 ms total loop delay (Figure 3.8). This 50 ms equivalent transport delay aggregates the 30 ms physical plant delay, identified during the system identification phase with a 20 ms buffer accounting for digital Zero-Order Hold

(ZOH), CAN bus communication latency and steering actuator dead-time.

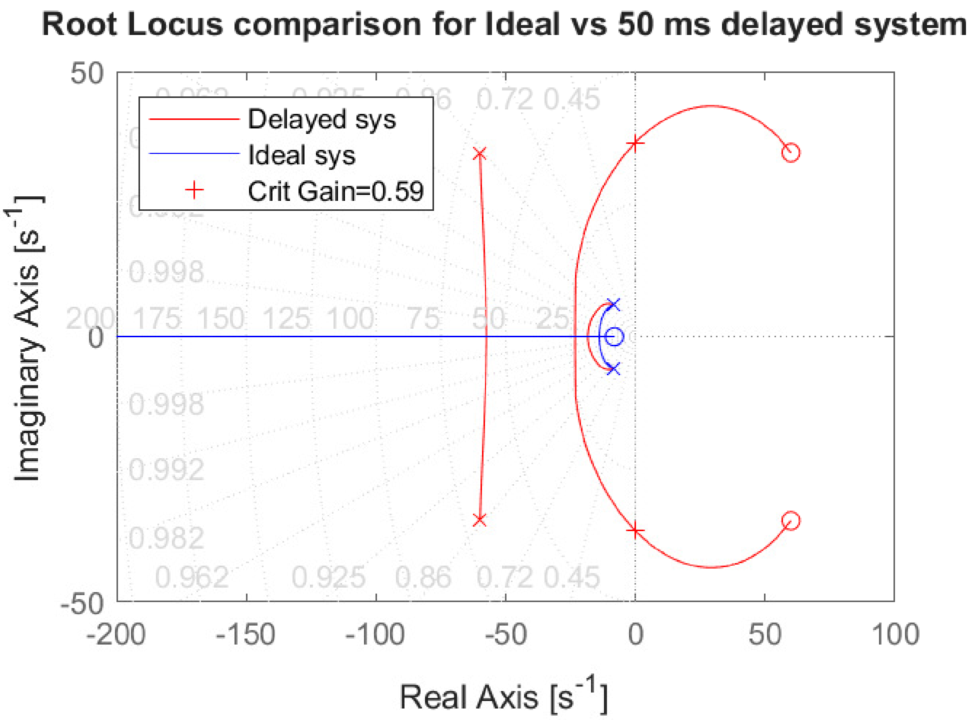

Figure 3.8: Root Locus comparison illustrating the shift of closed-loop poles for varying proportional gains. The hardware delay destabilizes the system, forcing the poles into the right half-plane at lower gain values.

As illustrated in the Root Locus plot, the introduction of the 2nd-order Padé approximated delay introduces right-half-plane zeros and significantly bends the dominant pole asymptotes toward the unstable right-half-plane. Consequently, the maximum stable theoretical gain is strictly limited to $K_p < 0.59$. Based on this delayed locus, a proportional gain of $K_p = 0.09$ was selected as base gain to ensure transient responsiveness while maintaining a large safe distance from the imaginary axis boundary.

3.3.2 Time-Domain Tuning and Trade-off Analysis

To observe how the theoretical stability boundaries translate into physical vehicle behavior, the yaw rate response was simulated using the validated linear single-track model. The simulated maneuver consists of a 2° road wheel steering step input to evaluate transient tracking, followed by an external lateral wind force 1600Nm to evaluate disturbance attenuation. To accurately reflect the physical hardware limitations, the identified 50 ms equivalent loop delay was incorporated into the closed-loop system.

Figure 3.9 demonstrates the open-loop response and closed-loop step response for three distinct proportional gains (K_p), while Figure 3.10 provides a detailed view of the overshoot and the subsequent stabilization phase.

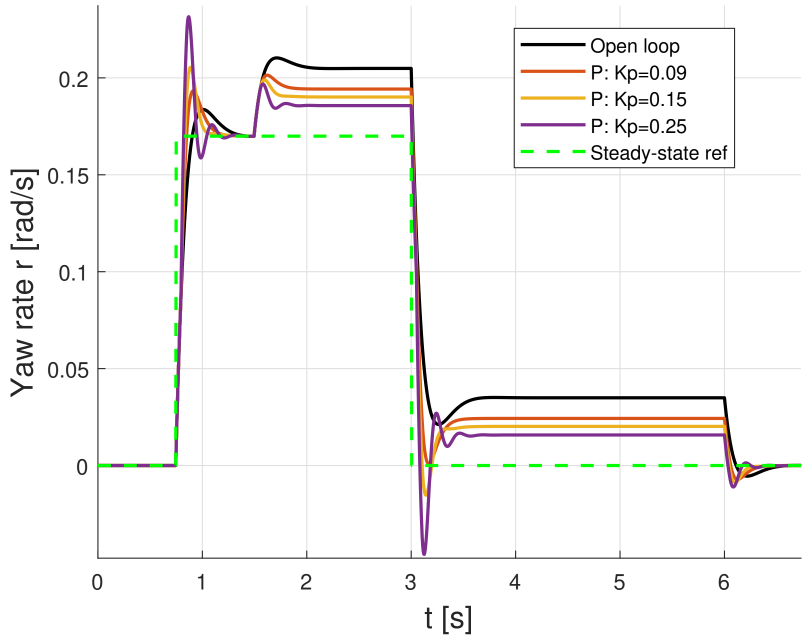

Figure 3.9: Simulated yaw rate step response and lateral wind disturbance attenuation for varying proportional gains (K_p) given a 50 ms actuation delay.

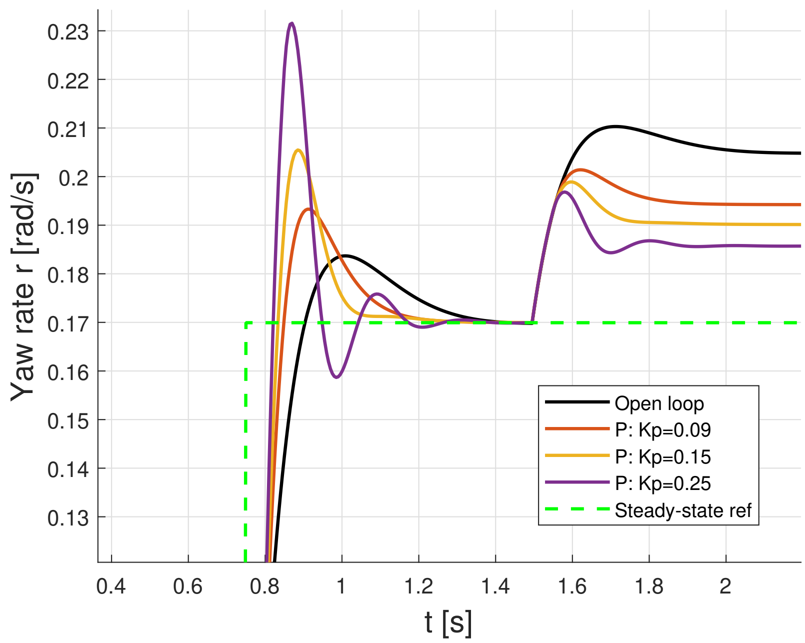

Figure 3.10: Detailed view of the simulated transient tracking response, illustrating the critical trade-off between rise time and delay overshoot.

The simulations illustrate the fundamental tuning trade-off caused by the system delays. A low proportional gain results in a slower tracking response and low suppression of the wind disturbance. On the contrary, a higher gain yields a faster initial rise time, but it forces the controller to act aggressively. Due to the combination of the 50 ms hardware actuation delay and the inherent dynamic phase lag of the vehicle causes the system to overcompensate, resulting in overshoot and oscillations.

Based on this time-domain analysis and Root locus analysis previously described, the proportional gain was established at $K_p = 0.15$. This configuration provided the best engineering compromise, delivering rapid transient stabilization and effective disturbance attenuation while maintaining sufficient damping to avoid instability induced by the combined system delays.

The PID controller variation was evaluated to observe the influence of the integral action. As illustrated in Figure 3.11, the inclusion of integral control proved highly dangerous. Because of the 50 ms delay and the vehicle natural inertia. Most noticeable during the constant wind disturbance the integral term continuously accumulate tracking error. By the time the vehicle reaches the reference yaw rate, the integral is wound up, forcing the controller to induce destabilizing overshoot to unwind the accumulated error when the wind disturbance stops. Consequently, the integral term was permanently discarded.

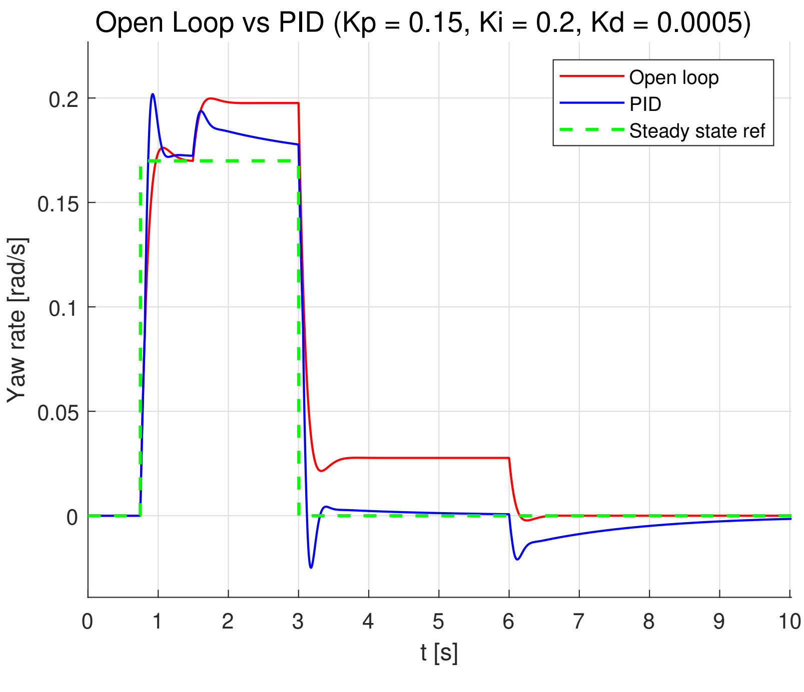

Figure 3.11: Simulated yaw rate step response and lateral wind disturbance attenuation for PID contoller given a 50 ms actuation delay. Showcasing the integral wind up.

Subsequently, the derivative term (K_d) was evaluated to determine if it could provide predictive damping. However, simulations revealed only marginal performance improvements that did not justify the added susceptibility to high-frequency sensor noise from the IMU.

3.3.3 LQR simulation

Following the P baseline evaluation, a time-domain analysis was conducted for the LQR controller. The simulation evaluated the systems step response and lateral wind disturbance attenuation across different configurations of the state-cost matrix (Q), specifically adjusting the penalty weights between the yaw rate and the side-slip angle. The results are showcased in Figure 3.12:

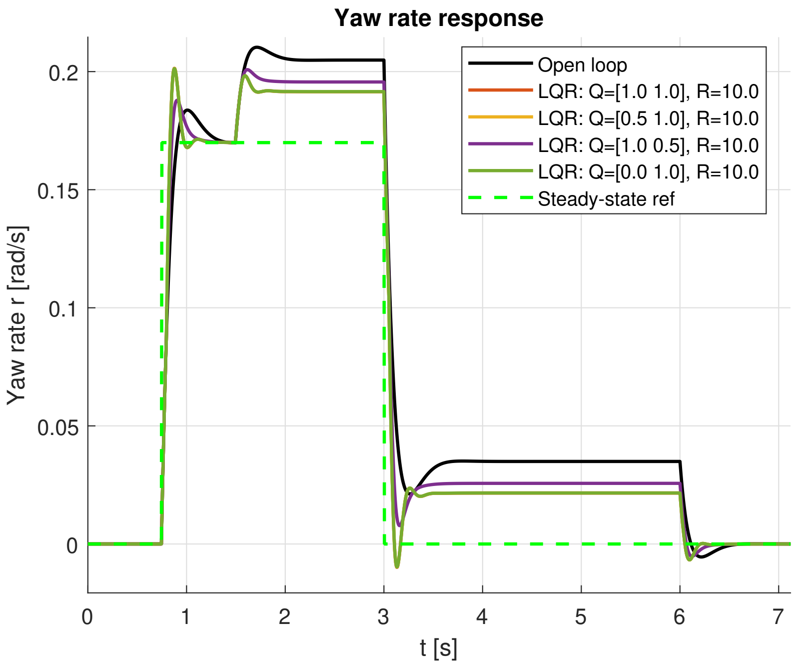

Figure 3.12: Simulated yaw rate step response and lateral wind disturbance attenuation for varying Q given a 50 ms actuation delay.

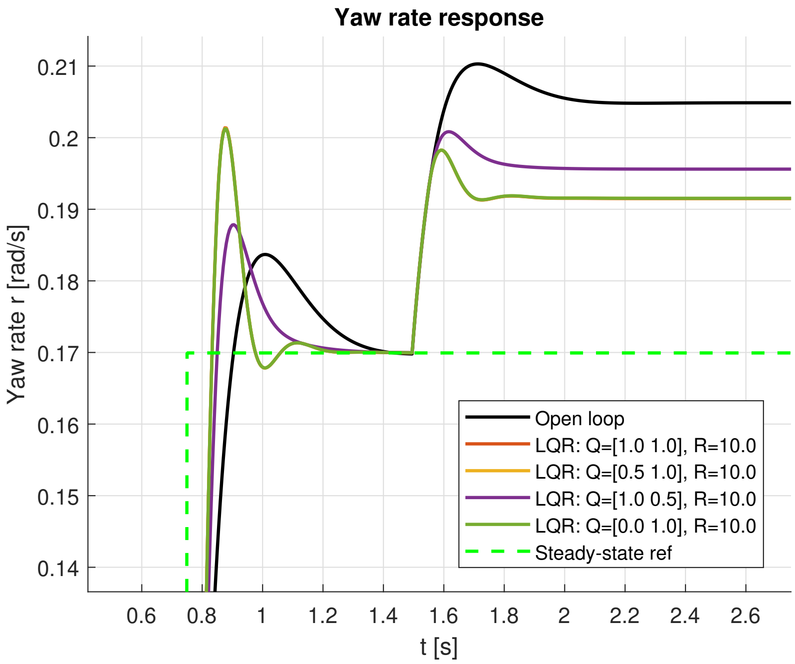

Figure 3.13: Detailed view of the simulated transient tracking response, illustrating the critical trade-off between rise time and delay overshoot.

As illustrated in the figures, the LQR provides transient performance comparable to the baseline proportional controller. Increasing the state weight on the yaw rate naturally improves tracking speed and minimizes the steady-state error. However, introducing a higher penalty on the side-slip angle inherently degrades the yaw rate tracking. This demonstrates a tradeoff in the optimal control design: by penalizing sideslip over aggressive yaw reference tracking, results in a more sluggish yaw rate response.

Since the primary objective of the active stabilization system is strictly to minimize yaw rate error, incorporating the unmeasurable β state provides no performance advantage for this specific task. The optimal multi-state LQR architecture therefore offers no tangible benefit over a standard single-variable controller. Consequently, the Proportional controller was selected for the final implementation.

3.3.4 RMS Values from Simulation

To quantitatively compare the efficacy of the different control strategies, the Root Mean Square (RMS) tracking error was calculated for the simulated maneuvers. The analysis evaluated the P, PD and various LQR configurations under the exact same conditions, including the 50 ms hardware delay.

Table 3.7: RMS tracking error comparison for the simulated controller architectures with a 50 ms loop delay.

Controller Architecture	RMS Tracking Error (rad/s)
Open-Loop Baseline	0.026118
P-Controller ($K_p = 0.09$)	0.020399
P-Controller ($K_p = 0.15$)	0.018536
PD-Controller ($K_p = 0.15, K_d = 0.0005$)	0.018434
LQR (Yaw-rate focused: $Q_r = 1.0, Q_\beta = 0.0$)	0.019049
LQR (Side-slip penalized: $Q_r = 0.5, Q_\beta = 1.0$)	0.020999

The results indicate that the PD controller achieves the lowest overall RMS tracking error, but by a marginal difference compared to the pure P controller. However, the pure proportional (P) controller demonstrated the most robust behavior against delay-induced high-frequency oscillations. Furthermore, while the LQR strategy regulates the side-slip angle, this competing multi-variable objective inherently increases the RMS error for the yaw rate.

As shown in Table 3.7, the active P-controller reduces the RMS tracking error from 0.0261 rad/s to 0.0185 rad/s compared to the unassisted baseline. While these absolute values may visually appear small because radians are a large unit for passenger vehicle yaw rates, this actually represents a substantial relative error reduction of approximately 29%.
This mathematical improvement is physically critical. The absolute RMS error reduction of approximately 0.0076 rad/s (or 0.43°/s) from the baseline to the P-controller is critical for high-speed tracking. At 80 km/h, an uncorrected yaw error of nearly half a degree per second will cause a vehicle to drift out of its lane within seconds. By successfully shortening transient yaw rate peaks during disturbances, the controller eliminates the need for steering micro-adjustments by the driver, translating this numerical reduction into a noticeably safer and smoother driving experience.
Consequently, The near identical RMS tracking errors between the yaw rate focused LQR and P controller provides confirmation of their theoretical equivalence. Furthermore, if the primary objective is strictly to minimize the yaw rate tracking error, the baseline P or PD architectures prove to be the most effective and robust approaches for this specific hardware configuration. Therefore, the architecture was simplified entirely to a pure Proportional (P) controller.

3.3.5 Frequency Domain and Robustness Analysis

The theoretical stability and robustness of the open-loop plant and the tuned closed-loop P-controller were evaluated using the metrics established in the methodology.

To quantify how much the physical system parameters can vary before instability occurs, the stability margins of the delayed open-loop system were evaluated through a

Bode response analysis. Figure 3.14 displays the amplitude and phase characteristics.

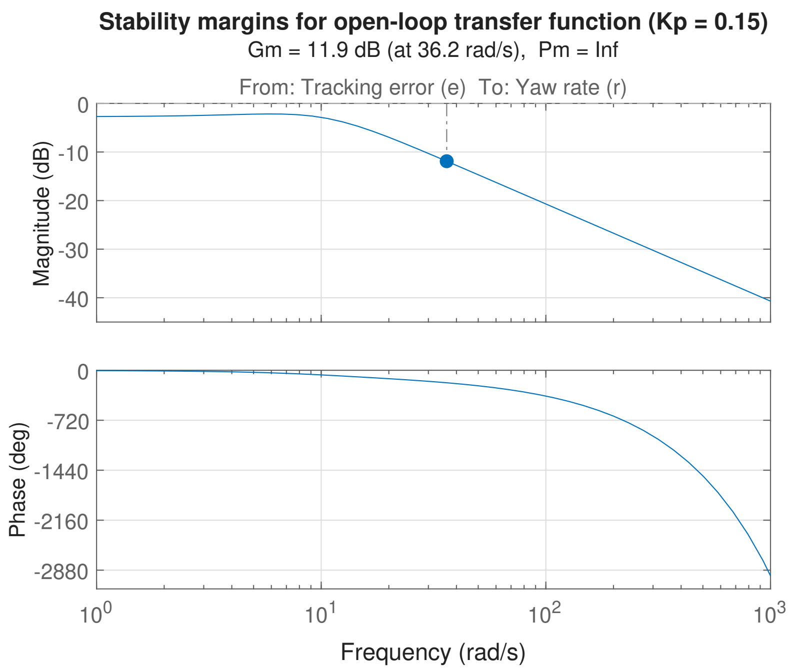

Figure 3.14: Bode plot of the delayed open-loop transfer function $L(s)$.

As illustrated in the Bode plot, the system achieves a Gain Margin of 11.9 dB at a phase crossover frequency of $\omega_{pc} = 36.2$ rad/s. The closed-loop system is confirmed to be stable, as the stability criterion defined in Equation 2.28 is successfully fulfilled:

$$AR_{OL}(36.2) = 0.2541 < 1 \tag{3.2}$$

The Bode analysis revealed a critical characteristic of the tuned architecture: the Phase Margin (PM) evaluates to infinity. This occurs because the open-loop steady state magnitude ($K_p \cdot G_{ss}$) always evaluates to less than 0 dB, regardless of the longitudinal velocity (v_x). This means the system gain remains strictly below the 0 dB amplification threshold across all frequencies. Consequently, a gain crossover frequency (ω_{gc}) does not exist.

From a physical standpoint, this proves that the open-loop signal is strictly attenuated. While high time delays will naturally degrade tracking performance and induce damped oscillations, the system lacks the open-loop signal amplification required to sustain a runaway positive feedback loop. Therefore, the theoretical maximum tolerable time delay (t_{max}) is strictly infinite, rendering the $K_p = 0.15$ configuration unconditionally stable against pure transport latency.
The absolute stability of the chosen P controller ($K_p = 0.15$) was further confirmed via the Nyquist plot in Figure 3.15.

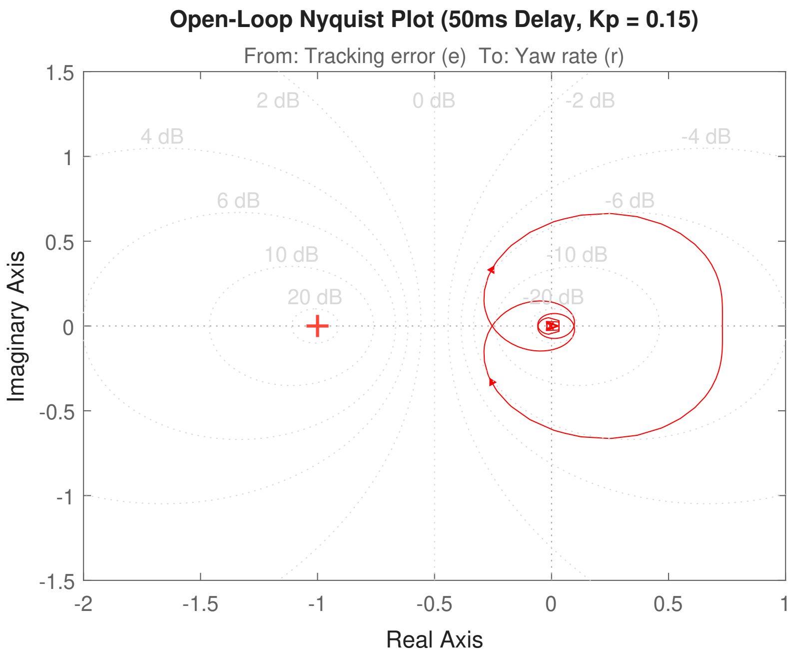

Figure 3.15: Nyquist plot of the delayed open-loop system.

As expected, the physical transport lag introduces a continuous phase shift at higher frequencies, causing the tail of the Nyquist contour to spiral outward toward the left half-plane. However, visual inspection confirms that this delayed trajectory safely bypasses and does not encircle the critical instability point $(-1, 0j)$, meaning $N = 0$. Given that the open-loop plant have no right half-plane poles ($P = 0$), the Nyquist criterion in Equation 2.30 mathematically guarantees absolute closed-loop stability for the physical SbW vehicle.

Finally, the system's robustness against external lateral disturbances and unmodeled high-frequency sensor noise was quantified using the Sensitivity function $S(s)$. Figure 3.16 illustrates the magnitude response of this function across the frequency spectrum.

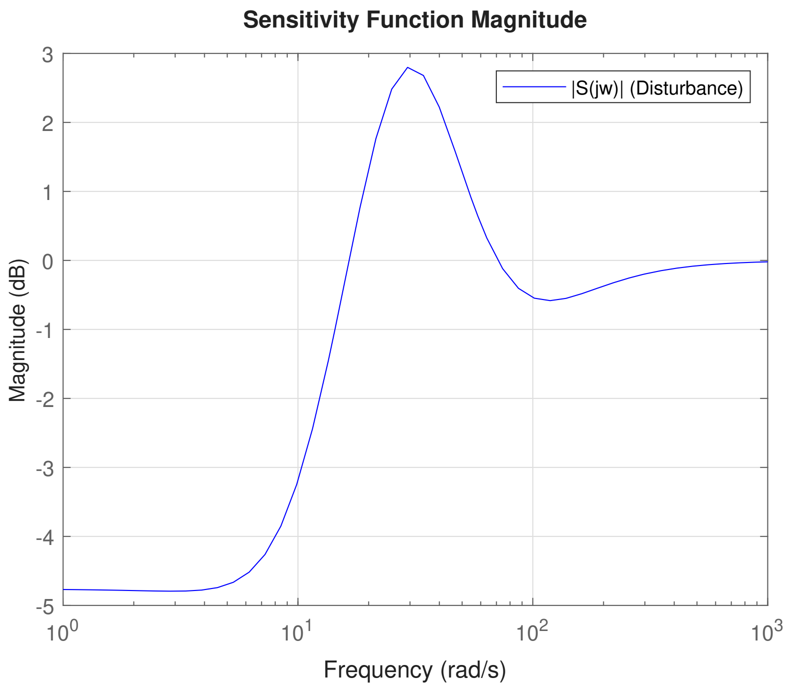

Figure 3.16: Magnitude of the Sensitivity function $S(s)$

As illustrated in the figure, the maximum sensitivity peak (M_s) evaluates to 1.38. This value falls perfectly within the established robust engineering target range of $1.2 \leq M_s \leq 2.0$. This confirms that the closed-loop system will effectively suppress lateral wind gusts without inducing severe shudder or amplifying high-frequency noise from the IMU.

3.3.6 In-Vehicle Robustness and Stability Limits

As established in the methodology during the tuning process, multiple driving tests were conducted to collect measurements and evaluate how the theoretical stability boundaries translated to the physical prototype vehicle. The objective of these tests was to confirm the robustness of the selected baseline gain and to physically observe the system's absolute instability limit. Figure 3.17 presents the time-domain telemetry from these tests, comparing the actual measured yaw rate and steering wheel angle across three different proportional gains.

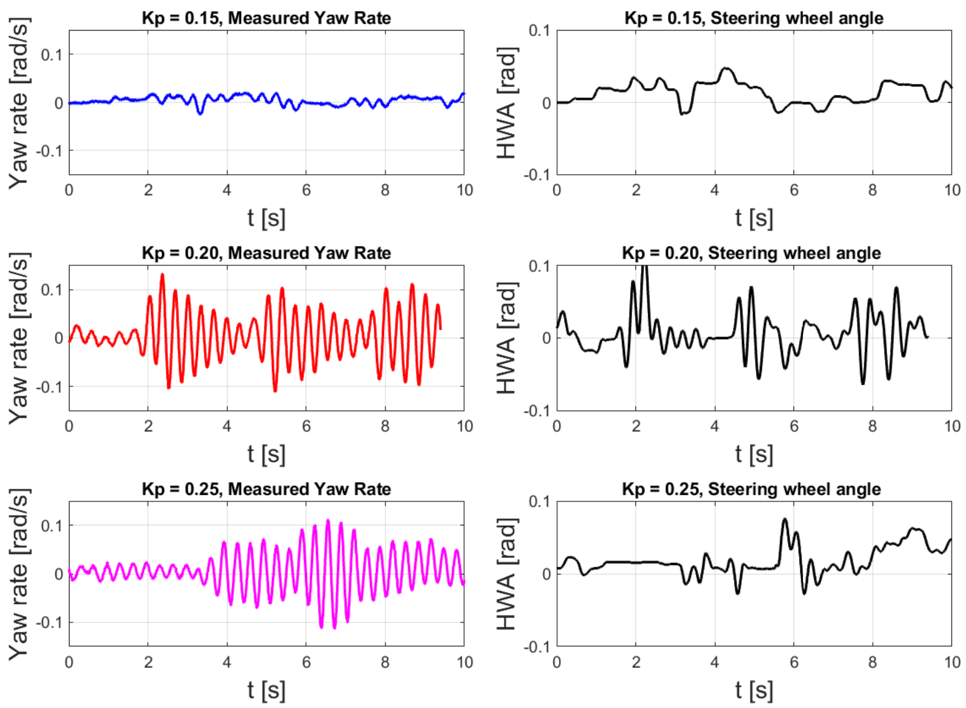

Figure 3.17: Real driving tests, illustrating oscillations and system instability when the proportional gain is increased.

The logged data clearly demonstrates the physical consequences of exceeding the stability threshold. While the system remained stable and predictable at the conservatively chosen baseline gain, progressively increasing the proportional gain (e.g., to $K_p = 0.20$ and $K_p = 0.25$) triggered oscillations. The practical results align with the simulated results and the chosen gain $K_p = 0.15$ was deemed robust.

3.3.7 Dynamic Lane Change Maneuvers

The transient tracking performance and dynamic damping capabilities of the active controllers were evaluated in the physical prototype vehicle during the lane change maneuvers. The actual measured yaw rate of the vehicle was compared against the reference ideal steady-state reference yaw rate.

Figure 3.18 presents the time-domain measured yaw rate response, steering input, vehicle speed for the baseline compared to the assisted system when the P-controller is active.

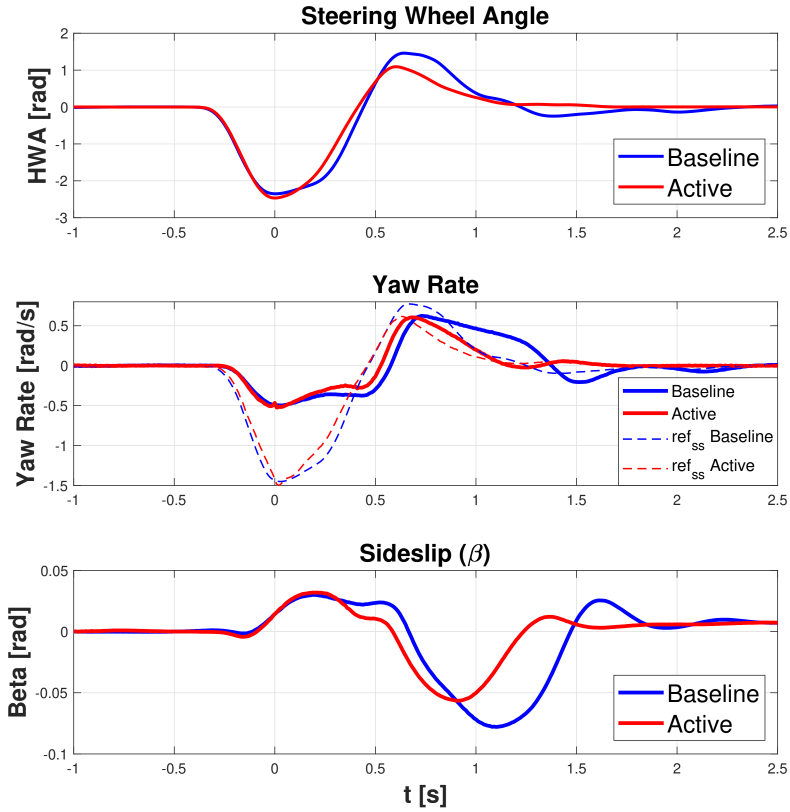

Figure 3.18: Measured vehicle yaw rate compared to the reference target during a high-dynamic lane change for baseline and assisted configuration

The time-domain data illustrates how both configurations initially fail to perfectly track the rapid step in the steady-state reference due to the inherent yaw inertia of the physical vehicle. However, during the transient overshoot of the second steering reversal, it is noticeable that the vehicle yaw rate is following the steady state reference significantly faster when the controller is active.
When the active controller is engaged the transient performance is visibly improved. The P controller successfully minimizes the tracking error and actively damps the yaw rate over-swing.

To verify the control input of the system, the corrective steering overlay (δ_{add}) was also analyzed. As shown in Figure 3.19, the measured steering overlay requested by the controller remained within the established safety constraint of $\pm 7°$ throughout the entire maneuver. However, as an consequence of the rapid turn and large tracking error at the initial turn, the request was capped at maximum even though the controller wanted to add more overlay than possible at $t = 0$.

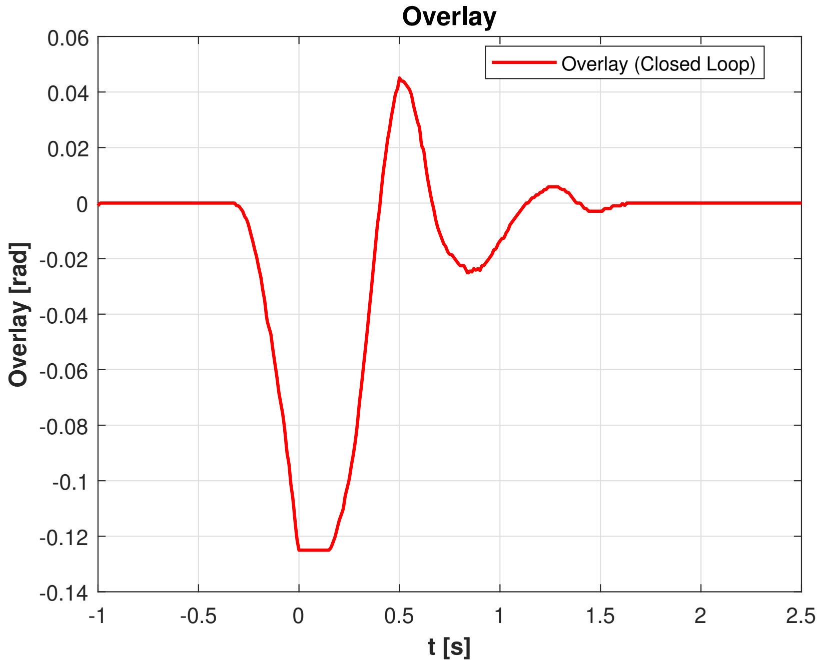

Figure 3.19: Measured active steering overlay (δ_{add}) applied by the controllers during the lane change maneuver.

Furthermore, to understand the operating region of the vehicle dynamics during this maneuver, the lateral acceleration (a_y) was recorded and is presented in Figure 3.20.

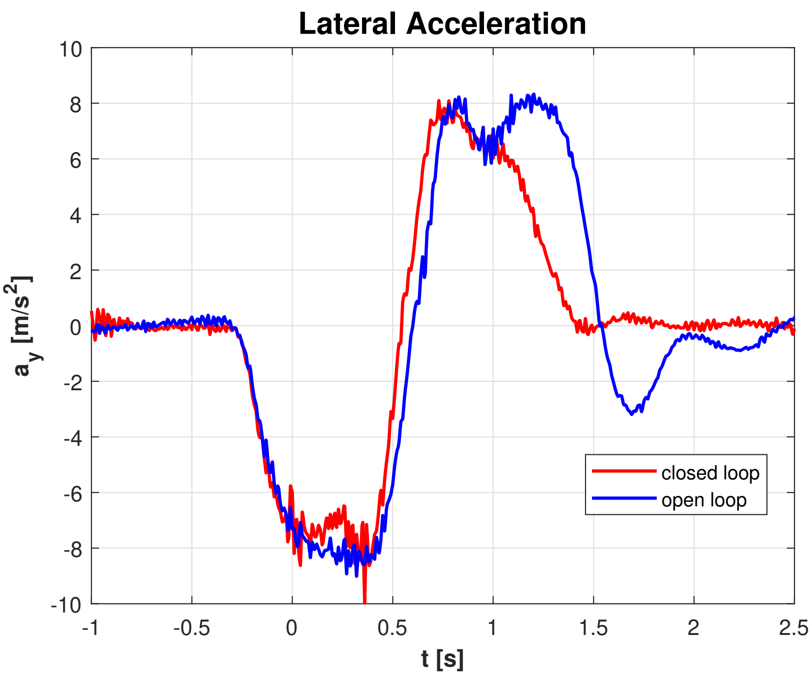

Figure 3.20: Measured lateral acceleration (a_y) during the lane change maneuver.

The aggressive nature of the maneuver forced the lateral acceleration to exceed 5 m/s^2 during the peaks of the maneuver. This meant that the vehicle transitioned out of the linear region assumed by the bicycle model, pushing the tires into their non-linear limits. Which explain the deviation between the reference model and the actual yaw rate in Figure 3.18.

Despite this model mismatch, the controller remained robust and improved the overall stability of the vehicle. Because the steering overlay stayed within the imposed $\pm 7°$ constraint and as established by the system's high theoretical stability margins (an infinite Phase Margin and a peak sensitivity of $M_s = 1.38$), the controller was able to safely overpower these unmodeled non-linear dynamics without inducing runaway high-frequency oscillations.As a result, the active intervention successfully accelerated the transient stabilization phase and damped the yaw rate over-swing much faster than the unassisted baseline configuration.

3.3.8 Disturbance Attenuation Tests (Trailer Towing)

The controller's disturbance attenuation capability was evaluated by towing a trailer under varying loading setups, as described in Section 2.5.2. The measured mass distributions for the two configurations are specified in Table 3.8.

Table 3.8: Measured corner weights (kg) for the vehicle and trailer. Configuration 1 represents a standard stable load, while Configuration 2 represents a severe rear-biased load.

Measurement Point	**Config 1 (Standard)**	**Config 2 (Rear-biased)**
Vehicle		
Front Left ($m1$)	624.5	636.0
Front Right ($m2$)	625.5	642.0
Rear Left ($m3$)	719.5	680.0
Rear Right ($m4$)	703.0	661.5
Trailer		
Left Wheel ($m1$)	342.0	367.5
Right Wheel ($m2$)	345.0	370.5

As observed in the measured data, transitioning to Configuration 2 significantly unloads the vehicle's rear axle ($m3$ and $m4$) while simultaneously increasing the load on the front axle ($m1$ and $m2$). This measurable weight transfer mathematically verifies the presence of a negative tow hook weight, deliberately forcing the trailer's CoG behind its own axle to introduce the instability required for the test.
The tracking performance was quantified by comparing the actual measured vehicle yaw rate against the steady-state reference. The distribution of the mean of RMS error, maximum peak error and phase delay across the test runs is illustrated as box-plots in Figure 3.21 for the baseline test using Configuration 1.

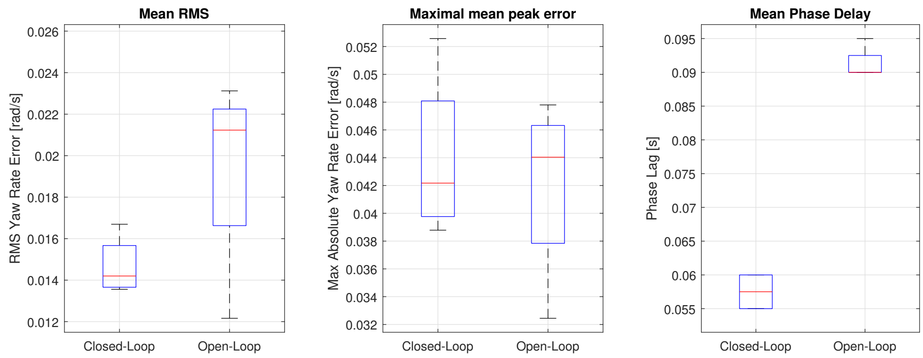

Figure 3.21: Boxplots illustrating the measured distribution of RMS error, peak error and phase delay during towing with the standard stable load (Configuration 1).

In this standard setup, the natural damping of the vehicle and trailer is sufficient to maintain stability. Neither the baseline system nor the active controller experienced any instability. However as shown in Table 3.9, the active controller still provided a measurable improvement in the overall tracking performance, notably reducing the mean phase delay by 37.0 % and the mean RMS error by 24.6 % despite a increase in the peak error.
The Mean Peak Error slightly worsened by 4.4 %. This increase is an expected trade-off when using a proportional controller in a system with hardware delays. When the driver makes a sudden steering input, the P-controller reacts aggressively to the large initial error. Because of the 50 ms delay, causing a brief overshoot past the reference target. This momentary overshoot is what creates the higher peak error. Despite this initial spike, the controller quickly dampens any subsequent trailer oscillations. As a result, the overall tracking performance across the entire maneuver is still better.

To evaluate the disturbance attenuation under severe conditions, the tests were repeated using the rear-biased setup (Configuration 2). The statistical distribution of the performance for these runs is presented in Figure 3.22.

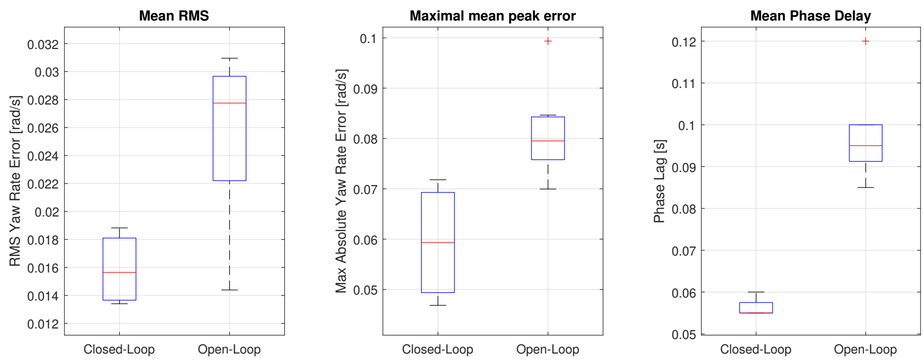

Figure 3.22: Boxplots illustrating the measured performance metrics when subjected to severe trailer sway induced by the negative tow hook weight (Configuration 2).

Table 3.9: Quantitative performance comparison between the baseline and the active closed-loop controller during the dynamic trailer towing maneuvers.

Performance Metric	Open-Loop	Closed-Loop	Improvement
Load Configuration 1 (Standard Load)			
Mean RMS Error (rad/s)	0.01944	0.01466	24.6 %
Mean Peak Error (rad/s)	0.04208	0.04393	-4.4 %
Mean Phase Delay (s)	0.091	0.058	37.0 %
Load Configuration 2 (Rear-Biased Load)			
Mean RMS Error (rad/s)	0.0252	0.0159	36.8 %
Mean Peak Error (rad/s)	0.0815	0.0593	27.2 %
Mean Phase Delay (s)	0.098	0.056	42.5 %

In the unassisted state without controller, the external lateral forces from the trailer loaded with configuration 2 were amplified compared to the configuration 1. When the controller is engaged, it successfully identifies the uncommanded changes in yaw rate and by applying corrective steering overlays, the system effectively restores the vehicle to a stable trajectory.
As detailed in Table 3.9, this active intervention resulted in a substantial improvement across all critical metrics compared to the open-loop baseline. The active controller reduced the mean RMS error by 36.8 % and decreased the dynamic phase delay by 42.5 %, statistically proving its effectiveness in suppressing delay-induced instability and maintaining vehicle composure during severe external disturbances.
Unlike the standard setup, the mean peak error was also improved by the controller in this configuration, showing that the controllers rapid intervention suppresses the disturbance caused by the Rear-biased loaded trailer.

3.3.9 Gravel Surface Testing

Through the subjective evaluation, data was recorded to investigate the controller capabilities in low friction gravel surface and its performance when the linear assumption of the car began to degrade. Testing on gravel surface cause chaotic, unpredictable steering corrections due to the driver attempts to stabilize the vehicle. Because of the non-repeatable nature of the driver's inputs across multiple runs, aggregating the time-domain data into an average trajectory does not yield a physically meaningful representation of the vehicle's dynamics. Therefore, the results are evaluated using a statistical analysis of the tracking error across all test runs to quantify overall performance by calculating RMS.

To quantify the controller's efficacy across varying degrees of maneuver severity, the RMS tracking error between the reference yaw rate and the measured yaw rate was calculated for all test runs. As established in Equation 2.22, the active steering overlay was explicitly subtracted from the primary road wheel angle prior to calculating the reference yaw rate. This ensured that the target trajectory strictly represented the driver's intended path, preventing the controller from artificially shifting its own reference target.

The statistical distribution of the RMS tracking error for both the baseline and the assisted system is presented in Figure 3.23.

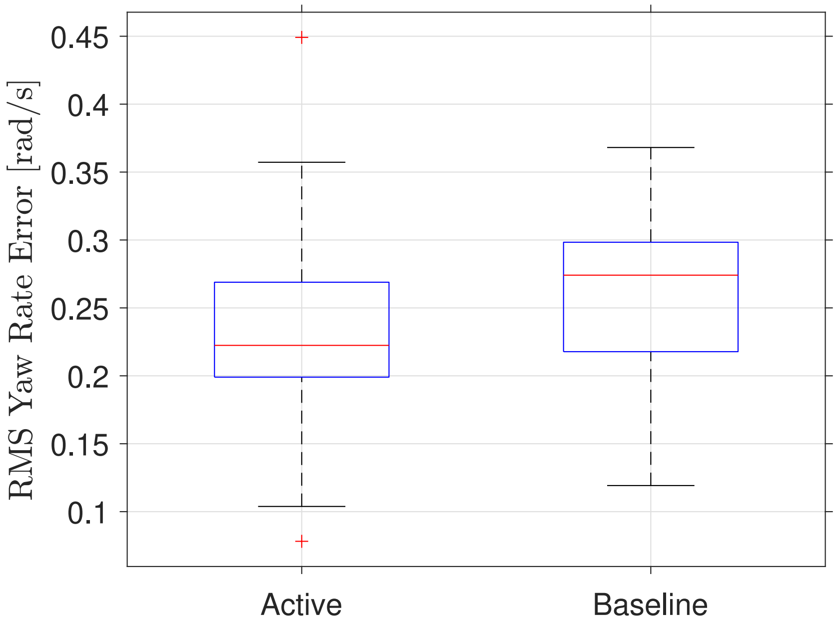

Figure 3.23: Distribution of the measured RMS tracking error for yaw rate tracking across all gravel test runs

The boxplot reveals an improvement in vehicle stability when the active controller is engaged. The closed-loop system achieved an 11% reduction in the mean RMS tracking error compared to the open-loop baseline. Visually, this is supported by the lower median error (indicated by the red line), proving that the proportional overlay successfully forced the vehicle closer to the linear reference model despite the saturated tire states. Furthermore, its interquartile range (the central blue box) is noticeably tighter. This compression of the core error distribution indicates an increase in vehicle consistency, meaning the controller made the vehicle's dynamic response much more predictable for the human driver across varied slip conditions.

3.3.10 Subjective Evaluation

To complement the objective telemetry data, a subjective evaluation was conducted. It should be noted that this was an informal assessment conducted primarily as a final check to measure driver feedback.
The drivers rated their experience on a 7-point scale (where 1 represents Strongly Disagree and 7 represents Strongly Agree). The questionnaire evaluated the system across three primary testing scenarios: driving on gravel surface, the trailer disturbance test and the standard dynamic lane change.

Out of the 12 invited drivers 8 people performed the evaluation and during the writing of this thesis only 5 people has answered the questionnaire, only 1 driver has answered question 5. Due to time limitation on the subjective evaluation day, responses was not collected exactly after the maneuvers were performed which could impact the evaluation. The average ratings for the specific metrics evaluated during each maneuver are consolidated in Table 3.10.

Table 3.10: Average ratings (1-7 scale) for the active controller. Question numbers correspond to the full evaluation form available in Appendix A.

Gravel Test	**Average Rating**
Q1. Reduced manual counter-steering compared to open loop	4.40
Q2. Intuitive control (did not fight driver inputs)	5.60
Trailer Test	**Average Rating**
Q5. Reduced manual counter-steering compared to open loop	7.00
Q6. Less perceived physical disturbances in the cabin	7.00
Q8. Controller interventions were smooth without jerks	6.67
Q7. Vehicle felt overall more stable	6.33
Lane Change Test	**Average Rating**
Q11. Stabilized quickly without unwanted oscillations	5.25
Q12. Intuitive control (did not fight driver inputs)	6.25
Q13. Controller interventions were smooth without jerks	6.25
Q14. Vehicle felt overall more stable	5.50

The trailer disturbance test yielded the most remarkable results, with test subjects reporting a surprisingly large difference in ride quality. Driver and passengers rated the reduction of physical disturbances at a perfect 7.00, noting that the controller significantly attenuated the disturbances from the trailer. Feedback strongly supported this, one passenger seated in the rear noted that the system made an "insane" difference, significantly reducing motion sickness and describing the ride as feeling like "flying on a magic carpet" when the controller was active compared to without.

For the standard single lane change maneuver, the system received high scores for smoothness (6.25) and intuitive control (6.25), indicating that the active steering overlays (δ_{add}) were successfully added without disturbing the driver's primary steering feel. In the written comments, participants highlighted that the maneuver required "less steering effort" and felt "less dramatic" particularly during the return phase of the lane change. While one driver found it "difficult to feel a clear difference in this driving scenario alone" the general feeling was that the vehicle felt significantly more composed and "tidy". One driver noted that the system prevented Electronic Stability Control (ESC) interventions that were otherwise sometimes triggered during the open-loop runs.

For the dynamic driving test on the gravel surface, the qualitative feedback was more nuanced. Because the low-friction surface forces the vehicle into its non-linear limits, some drivers noted that the vehicle occasionally felt unpredictable to them as experienced drivers. Their natural instinct to manually counter-steer sometimes conflicted with the active controller's rapid interventions. One evaluator stated that an experienced driver "would like to opt out of this controller setting if possible". Conversely, the same feedback emphasized the system's objective safety benefit, noting that "for the average driver this controller would make it significantly safer since it controls the drift in a stable way."

Furthermore, another driver observed a positive interaction with the vehicle's traditional safety systems, they noted that when the vehicle started to drift and the brake-based ESC was eventually activated, the transition felt significantly smoother and less aggressive compared to the baseline without the controller assistance. These subjective observations align perfectly with the dynamic telemetry, confirming that while the linear reference model may struggle with extreme non-linear conditions, the active steering intervention still effectively assists in damping transient instability faster than humanly possible while softening the harshness of subsequent brake-based interventions.

3.3.10.1 Overall Controller Preference

After each specific test scenario, the drivers were explicitly asked whether they preferred driving the maneuver with the active controller engaged or in the unassisted open-loop configuration.

Figure 3.24-3.26 illustrates the overwhelming preference for the active yaw rate stabilization system. During the trailer and lane change maneuvers, 100% of the respondents preferred the active controller. In the gravel test, 80% preferred the active system, with a minority preferring the unassisted vehicle.

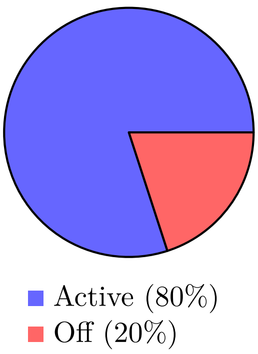

Figure 3.24: Gravel Test

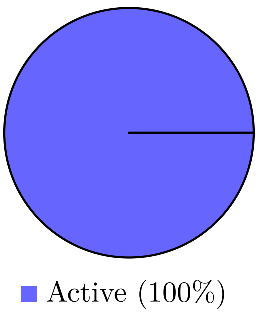

Figure 3.25: Trailer Test

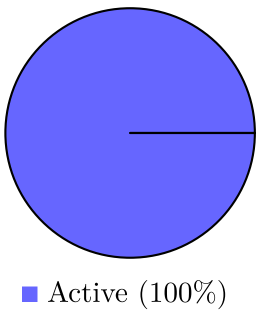

Figure 3.26: Lane Change Test

4

Discussion

4.1 Reference Model Validity and Safety Margins

The linear single-track (bicycle) model was selected to represent the undisturbed, ideal vehicle response. While this model serves as a robust baseline, incorporating roll and pitch dynamics into a more advanced two-track model would fundamentally improve the theoretical accuracy of the reference generator. Specifically, including roll dynamics would capture lateral load transfer during cornering, which alters the effective cornering stiffness of the tires. Similarly, pitch dynamics would account for longitudinal weight transfer if the driver were braking or accelerating during a maneuver.

However, these advanced models introduce a significant increase in computational complexity and require real-time estimation of states such as individual tire vertical loads and suspension deflection which are difficult to observe reliably using standard production vehicle sensors. Therefore, the single-track model was retained as it offers an optimal balance between sufficient predictive accuracy and robust real-time performance for embedded SbW control systems.

An essential component of this model was the accurate parameter estimation of the understeer gradient (K_{us}). An accurate baseline for this parameter fundamentally dictates the vehicle's ideal steering feel. Extracted from empirical track data, this model successfully captured the vehicle's fundamental lateral dynamics. Within its intended envelope (lateral accelerations below 5 m/s^2), the model proved highly accurate, achieving an 88.9% NRMSE fit on the validation dataset.

Frequency-domain validation also confirmed that the model successfully captured the dynamic bandwidth and high-frequency roll-off of the physical vehicle. A static gain offset at low frequencies was identified which can be due to the rigid chassis assumption of the bicycle model and the coupling constraint between front and rear cornering stiffnesses through the understeer gradient.

The higher NRMSE fit on the independent validation dataset is a consequence of the highly constrained nature of the grey-box identification. Because the physical model structure was fixed by the bicycle model equations and only a two free parameter C_f and I_z was optimized, the risk of overfitting to the estimation data was minimal. Furthermore, the estimation dataset contained aggressive steering inputs designed to excite the vehicle dynamics across the full 0.2 to 2.0 Hz frequency range, which pushed the vehicle closer to the boundaries of the linear model assumptions. In contrast, the validation dataset consisted of more natural and varied driving maneuvers, which fell more comfortably within the linear operating range of the model, resulting in a higher fit percentage.

However, from a vehicle dynamics perspective, a known theoretical limitation of the linear single-track model is the assumption of a rigid chassis and strictly linear tire forces. Consequently, the model ignores tire load sensitivity (lateral load transfer) and the suspension effect on the yaw rate and roll sensors. In reality, these phenomena cause the vehicle's true understeer gradient to vary depending on the nature of the maneuver and the time allowed for the chassis to settle into a steady state.

It is critical to acknowledge that the linear assumptions fundamentally break down during severe, non-linear events, such as driving on low-friction surfaces or executing extreme evasive maneuvers like when the lane change maneuver was executed. If the physical vehicle enters this non-linear region, the linear reference model could calculate an impossible target yaw rate that the physical tires mathematically cannot generate. Consequently, the controller will continuously increase the steering overlay in an attempt to reach the target. This overcompensation saturates the front tires, potentially exacerbating understeer, a phenomenon that was practically experienced during testing on the low-friction basalt track.

Despite this limitation, the controller still demonstrated practical value outside the strictly linear envelope. Results from the gravel track testing revealed that the active system reduced the tracking error and helped the drivers stabilizing the car much faster. This suggests that while the reference model may overestimate the achievable yaw rate in non-linear conditions, the controller's rapid interventions still effectively assist in damping transient instability faster than ordinary driver.

Furthermore, the frequency-domain robustness analysis mathematically proves that this linear reference is entirely sufficient for stable closed-loop control in the presence of real world disturbances. Because the tuned proportional controller ($K_p = 0.15$) achieved an infinite theoretical Phase Margin and a peak sensitivity (M_s) safely within the 1.2 to 2.0 threshold, the closed-loop system is mathematically guaranteed to suppress discrepancies between the linear model and the non-linear physical car. The control architecture possesses a robust enough safety margin to safely overpower unmodeled high-frequency dynamics, allowing the simplified reference model to dictate the intended vehicle posture without risking instability.

4.1.1 Sensitivity to Parameter Variations

The reference model and the nominal understeer gradient were estimated based on a specific baseline configuration: the vehicle's weight including the driver and one passenger, equipped with winter tires. However, in real-world deployment and even throughout the physical testing phases of this research, a vehicle's inertial and friction parameters are subject to significant variation.

A critical parameter affecting the understeer gradient is the cornering stiffness of the tires (C_f and C_r). Beyond the simple binary of summer versus winter compounds, a tire's cornering stiffness is continuously altered by its specific model design, seasonal ambient temperatures and depth. The relationship between tire's slip angle and the lateral force highlighted in Equation 2.6, Winter tires require larger slip angle to generate the same lateral force as the summer tires due to their inherently lower cornering stiffness.

To quantify this difference, steady-state circle testing was conducted using summer tires (two repetitions in each direction). The empirical data confirmed that the summer tires generated a slightly lower K_{us} value compared to the winter tires. Looking at the understeer gradient formula (Equation 2.12), this aligns perfectly since summer tires have larger values for C_f and C_r. The higher cornering stiffness allows the vehicle to generate required lateral forces at lower slip angles, reducing the overall understeer gradient and making the vehicle more responsive.

This physical discrepancy impacted the dynamic track evaluations, as the tests for the controller performance (excluding the regular road lane change) were executed with summer tires while the controller continued to utilize the K_{us} value obtained from the winter tires. According to the steady state yaw rate formula (Equation 2.11), larger understeer gradient value results in lower reference yaw rate. Because the vehicle on the summer tires turned faster than this yaw rate reference, the controller interpreted this as a tracking error and applied a appropriate overlay angle to compensate for the difference. Essentially, the controller safely constrained the agile summer-tire setup, forcing it to mimic the more conservative, understeer heavy trajectory of the winter tire baseline.

Similarly, variations in vehicle mass (m) and the CoG heavily dictate understeer behavior. A fully loaded vehicle with passengers or cargo in the rear shifts the CoG backward. Geometrically, this decreases the distance from the CoG to the rear axle l_r and increases the distance to the front axle l_f. Looking at Equation 2.12, making l_r smaller and l_f larger results in lower K_{us} value. Furthermore this rear focused weight increase the vertical load on the rear tires. Due to tire load sensitivity, a heavier tire become less efficient and needs larger slip angle to generate the same lateral force (see Equation 2.6). Both the geometric shift and the non-linear tire loading causes a decrease in the understeer gradient, shifting the vehicle's natural handling balance closer to oversteer.

This theoretical phenomenon was practically relevant during the testing phase, as several maneuvers were conducted with an additional experienced test driver in the vehicle. The added mass and rearward CoG shift theoretically made the physical vehicle more prone to oversteer. However, just as with the summer tire variation, the closed-loop controller actively suppressed this physical shift by continuously minimizing the error against the static, baseline reference model, ensuring consistent and predictable vehicle behavior regardless of passenger occupancy.

Ultimately, if the physical vehicle becomes highly responsive due to summer tires, or less understeery due to a shifted payload, the error calculated by the reference model changes rapidly. However, the theoretical robustness analysis guarantees that the closed-loop system can safely tolerate these physical changes without requiring real-time recalibration of the model.

Specifically, the Bode analysis revealed a Gain Margin of 11.9 dB. From a physical standpoint, this means the overall open-loop gain of the system which encompasses the cornering stiffness of the tires and the mass of the vehicle, can be multiplied by a factor of nearly 4 before the control loop becomes unstable. Therefore, even if summer tires and a shifted payload drastically increase the physical plant's responsiveness, the proportional controller ($K_p = 0.15$) is mathematically robust enough to attenuate the error without inducing dangerous high-frequency oscillations. Despite the static reference model being tuned for a baseline winter configuration, it remains a safe and reliable target generator for the controller across a wide range of physical payloads and tire conditions.

4.2 Hardware limitations

The performance of the lateral stabilization system was fundamentally bounded by the physical limitations of the SbW system configuration. The most prominent constraint was the identified total 50 ms actuation and communication delay. As demonstrated in the frequency domain analysis, this pure time delay introduced significant phase lag, forcing a reduction in the proportional gain to maintain an adequate stability margin. Consequently, the controller could not be tuned as aggressively as a continuous-time theoretical model permit, ultimately sacrificing some transient reaction speed for guaranteed safety.

Furthermore, the resolution of the corrective overlay signal (δ_{add}) was limited to an 8-bit integer over the CAN bus, resulting in discrete steering steps of approximately $0.056°$. While this quantization was sufficiently small to avoid noticeable jerks in the steering rack, it technically introduces a low-level quantization noise that limits the precision of micro-corrections during high-speed, steady-state driving where even minimal steering angles translate into significant lateral forces.

Finally the physical overlay steering action was strictly limited to maximum road wheel angle of $\pm 7°$. If the vehicle encounter a severe tracking error that mathematically requires a corrective overlay that exceeds this limit, the actuator saturates. This limitation further validates the decision to avoid integral action in the controller design which would have caused violet counter steering. By utilizing a pure proportional controller, the system safely saturates at the angle limit without accumulating previous errors ensuring predictable recovery when the vehicle returns to the linear range.

4.3 Controller implementation

The question of which control architecture is most suitable for this application was approached through two independent analytical paths, a systematic evaluation of classical PID components and an investigation of optimal state feedback through LQR. Critically, both paths converged on the same conclusion through different reasoning, providing strong theoretical justification for the final architecture selection.

Although a full PID structure was initially considered, the integral and derivative terms were intentionally kept out after the controller simulation. Integral action was highly susceptible to integrator windup during sustained disturbances and introduced phase lag. Furthermore, the vehicle operates as a human-in-the-loop system. The human driver naturally and intuitively compensates for minor steady-state tracking errors, rendering the mathematical integral term redundant. The derivative term was omitted because there was no noticeable improvement compared to only constant gain and because real-world yaw rate sensors contain high-frequency noise. Implementing a derivative controller would amplify this noise, necessitating aggressive low-pass filtering which would introduce additional phase delays to the already delayed system.

The LQR analysis approached the architecture selection from an optimal control perspective. The full two-state formulation requires feedback from both the yaw rate and the sideslip angle. While β can be estimated using advanced state observers to mitigate sensor drift, integrating such estimators was considered outside the immediate scope of this study. More importantly, the simulation results demonstrated that regulating multiple states using only a single control input (δ_{add}) inherently creates competing objectives. Penalizing the side-slip angle successfully restricts β but simultaneously degrades the yaw rate tracking performance.

While various methods exist to iteratively tune the state-penalty matrix Q and control effort R, the analysis concluded that the multi-variable LQR approach did not provide a tangible performance benefit for this specific application. The added complexity of state estimation and optimal tuning was ultimately deemed unwarranted given the primary objective. By contrast, the single-variable P controller provided direct regulation of the yaw rate and its tuning process was analytically driven by leveraging frequency domain techniques.

Most importantly, the LQR's theoretical optimality relies on the assumption of instantaneous state feedback. However, the inherent system delays cause its stability margins to degrade. Conversely, the P controller gain was mathematically capped at 0.15 to ensure the system never amplifies delayed, out-of-phase signals.
Finally, the P controller effectively addressed the requirement for crosswind disturbance attenuation. As proven by the sensitivity analysis, the peak sensitivity was kept within the robust target range. This ensures that the P controller will add overlay angle correction to suppress lateral wind gusts without inducing high frequency shuddering.

Future iterations could resolve these architectural limitations by implementing state observers alongside a threshold-based LQR, where the β-penalty is normally zero but activates exponentially only when the side-slip exceeds a critical safety limit. This would preserve tire grip without compromising daily driving dynamics. However, for the current hardware constraints, the model-free P controller provided the most effective, easily verifiable and robust solution.

4.4 Driving angled road

A notable consequence of relying on a planar bicycle model for the reference yaw rate (r_{ref}) is the system's behavior on laterally angled surfaces. The current implementation interprets any uncommanded yaw motion as a disturbance that must be rejected.

On a straight but heavily cambered road, the gravitational component acts as a lateral force pulling the vehicle sideways. Here, the controller successfully identifies the drift as a disturbance and automatically applies a corrective steering overlay. This is highly beneficial as it reduces the driver's need to constantly counter-steer, thereby reducing driver fatigue.

However, a conflict arises on banked curves specifically designed to assist the vehicle through a turn. In a perfectly banked curve, the lateral forces are balanced and the vehicle will naturally follow the curve even if the driver holds the steering wheel straight ($\delta_{driver} \approx 0$). Because the current reference model assumes a flat road surface, it will calculate a target yaw rate of $r_{ref} = 0$. The active controller will consequently interpret the vehicle's natural, intended cornering as a disturbance and erroneously apply an outward counter-steering overlay, fighting the road geometry. To fully resolve this in a production vehicle, the reference model would need to be expanded to include road bank angle estimations, likely utilizing a combination of lateral acceleration sensors and suspension travel data.

4.5 Electronic Stability Control vs Steer-by-Wire

Traditional Electronic Stability Control (ESC) systems monitor vehicle states and intervene primarily when the vehicle approaches its physical limits of adhesion, typically characterized by severe side-slip angles (β). When a critical instability threshold is breached, ESC applies asymmetric braking forces to individual wheels to generate a corrective yaw moment. While highly effective at preventing spin-outs in emergency situations, these brake-based interventions are inherently discrete. Furthermore, they bleed off longitudinal velocity and are often perceived as harsh or intrusive by the driver.

In contrast, the SbW active yaw rate disturbance attenuation controller developed in this thesis operates continuously within the linear handling region. The major difference between the two systems lies in the precision of the actuator. Since steering is physically a better method for influencing vehicle yaw dynamics than asymmetric braking. Therefore, the main vehicle dynamics contribution of this thesis is the utilization of the SbW actuator as a continuous yaw rate correction channel. Because the active overlay utilizes the precise, high-bandwidth capabilities of the SbW actuator and acts on the same physical input used by the driver, the system can make extremely fine adjustments. Consequently, the intervention remains small, early, and continuous, as opposed to the discrete, threshold-based, and highly noticeable activations characteristic of ESC. As demonstrated in the results, the controller is fast enough to damp transient overshoots the moment they begin to develop.

By acting earlier and continuously regulating the yaw rate in the transient phase, the system reduces yaw rate deviations in a region where steering intervention remains smooth and acceptable. While the controller does not mathematically target the side-slip angle, rapid yaw rate correction physically bounds the vehicle's lateral motion. This effectively prevents the vehicle from building up the severe side-slip angles that would normally trigger an ESC intervention. This early steering approach not only preserves the vehicle's momentum which is particularly beneficial during continuous highway driving and trailer towing but also results in a significantly smoother driving experience.

Ultimately, the results indicate that steering-based yaw rate correction should not be viewed as a replacement for brake-based stability control near the handling limits. Instead, it serves as a highly effective, complementary system, it acts as a first line of defense to keep the vehicle stable within its linear envelope, reserving the coarse, brake-based ESC interventions exclusively for extreme non-linear emergencies. Furthermore, subjective feedback from the dynamic gravel testing confirmed that this complementary relationship actively improves the transition into ESC interventions. As noted by one of the test drivers, when the vehicle's slip eventually triggered the ESC, the brake-based intervention felt significantly smoother and less aggressive compared to the unassisted baseline runs.

4.6 Subjective Evaluation and System Boundaries

The subjective evaluations strongly corroborate the objective telemetry, while also highlighting the practical boundaries of the control architecture. The perfect 7.00 scores for disturbance reduction and the 100% driver preference during the trailer maneuver validate the core hypothesis of this thesis.
Conversely, the 80% preference split and the feedback from the gravel testing reveal the fundamental limits of relying on a linear reference model. On low-friction surfaces, the assumption of a constant understeer gradient (K_{us}) breaks down. The reference model calculates an ideal target yaw rate based on a high-friction baseline, but the reduced tire-road friction cannot physically achieve this trajectory. As a result, the controller interprets the lack of rotation as an error and continues to add corrective steering angle (δ_{add}), which risks saturating the front tires.
This physical saturation explains the conflict reported by experienced drivers. An

expert driver's natural instinct during a slide is to manually counter-steer and manage the slip angle, when the active controller intervenes rapidly to force the vehicle back to an impossible mathematical reference, it feels unpredictable and restrictive to the driver. However, the fact that the system still retained an 80% preference and was noted to make the vehicle "significantly safer" for average drivers proves that the system remains beneficial even outside its design linear range. The controller acts as an active damping force that stabilizes the drift and smooths the eventual transition into ESC.
It must be acknowledged that this subjective evaluation relies on a limited sample size of five respondents, which restricts broad statistical generalization. Nevertheless, the qualitative insights validate that the current architecture safely manages macroscopic body disturbances for the average driver.

5
Conclusion

The SbW technology represents a fundamental shift in vehicle dynamics, decoupling the physical mechanical connection between the steering wheel and the road. The primary purpose of this thesis was to design, implement and physically validate a closed-loop active steering controller capable of minimizing external lateral body disturbances without interfering with the driver's intended trajectory.

5.1 Reference Model and System Identification

Addressing the first research question, the linear single-track model proved to be highly effective at reliably predicting the vehicle's ideal steady-state yaw behavior. Parameterized using empirical track data, the model demonstrated strong predictive accuracy with an NRMSE fit of 88.9% against an independent validation dataset and successfully captured the vehicle's lateral dynamics within the defined linear operating region of lateral accelerations less than 5 m/s^2.

Frequency-domain stability analysis of the full closed-loop system further confirmed that this linear baseline constitutes a sufficient reference generator for stable closed-loop yaw rate control. While the linear assumptions inherently break down during extreme maneuvers where tires operate outside their nominal range, the system's stability margins are large enough to contain such model discrepancies without inducing instability. This confirms that a simple reference model serves as a highly practical baseline, improving overall vehicle predictability without requiring an overly aggressive control law.

5.2 Control Architecture Selection

In addressing the second research question, the study concludes that a model-free Proportional (P) controller is fundamentally better suited for this specific hardware configuration than a MB LQR. Attempting to regulate both the yaw rate and the unmeasured side-slip angle (β) with a single, delayed control input created competing objectives, which naturally degraded tracking performance. By removing the side-slip penalty to focus strictly on yaw rate tracking, the LQR essentially devolves into a standard P-controller.

Consequently, the pure P-controller was implemented as the optimal engineering compromise. It explicitly avoided the integrator windup associated with actuator saturation and prevented the amplification of high-frequency IMU noise that a derivative term would introduce. This architecture mathematically guaranteed absolute system stability against the physical 50 ms transport lag.

An overlay angle was generated by the controller whenever a yaw disturbance was detected. The overlay angle was added to stabilize the vehicle and to help reach the steady state faster. Furthermore the controller was optimized to operate safely withing a strict $\pm 7°$ mechanical constraint on the steering overlay.

5.3 Controller Performance and Analysis

Dynamic testing demonstrated that the controller successfully improves both disturbance attenuation and vehicle responsiveness compared to the unassisted baseline SbW. The most quantitatively compelling evidence was the trailer towing evaluations, where the controller demonstrated that its effectiveness scales with the severity of the disturbance. As shown in the rear-biased trailer towing, the controller achieved a reduced RMS yaw rate tracking error of 36.8% and 42.5% less mean phase delay. By acting as a continuous yaw rate correction channel, the system identifies yaw moment disturbances early and applies immediate, small corrective overlays. Because the reference target is defined solely by the driver's commanded steering input, the controller supports the intended path, successfully preserving driver authority even during rapid steering reversals.

Furthermore, the controller demonstrated excellent robustness under model mismatch. When tested with summer tires, the controller interpreted the vehicle's increased agility as a tracking error and applied corrective overlays that effectively constrained the vehicle to follow the more conservative winter-tire reference trajectory. Similarly, variations in passenger occupancy that shifted the CoG were continuously suppressed by the closed-loop error minimization, ensuring predictable vehicle behavior regardless of loading conditions without the need for system re-identification. These results are supported by the frequency-domain robustness analysis.

Subjective evaluations strongly corroborated the dynamic telemetry. The active controller achieved a 100% driver preference in standard handling and trailer towing scenarios which largely mimic the body disturbances cause by side wind. During extreme low-friction (gravel) testing, the system maintained an 80% preference by effectively smoothing the transition into ESC interventions and stabilizing drift for the average driver.

Ultimately, this research confirms that the closed-loop SbW controller constitutes an effective, robust first line of defense against lateral disturbances. By reacting continuously within the linear handling region, the system preserves vehicle composure and stability well before the coarse, brake-based interventions of traditional ESC become necessary.

5.4 Future Work

While the implemented proportional controller successfully demonstrated the potential of active SbW yaw rate stabilization, there are several areas for future development.

Gain Scheduling and Velocity Adaptation: The current controller utilizes a static proportional gain ($K_p = 0.15$) optimized for highway speeds (80 km/h). However, vehicle yaw damping inherently increases at lower velocities. Future implementations should incorporate a gain-scheduled approach, dynamically scaling the feedback gain as a function of longitudinal velocity (v_x) to maintain mathematically optimal stability margins and maximize responsiveness across the entire speed range.

Advanced Reference Modeling for Road Geometry: The current planar single-track reference model assumes a perfectly flat driving surface. Consequently, the controller interprets the natural gravitational forces of a banked curve as an external lateral disturbance, erroneously applying an outward counter-steering overlay to resist it. Future implementations should upgrade the internal reference generator to a more advanced mathematical framework, such as a dual-track model incorporating roll dynamics and nonlinear tire behavior.

Extended Multi-State Control Objectives: The present study utilized yaw rate as the sole feedback target. Future work could extend the control architecture to jointly consider yaw rate alongside lateral acceleration, lateral velocity, or sideslip angle. This multi-variable approach would enable a more complete and precise control over the vehicle's macroscopic body motion.

Explicit Coordination with Brake-Based Stability Control: While the current active steering overlay naturally serves as an early, continuous defense mechanism that smooths the transition into eventual ESC interventions, there is no active communication between the two systems. Future architectures should develop explicit software coordination between the SbW controller and brake-based stability systems.

Integration of Long-Term Steady-State Compensation: Integral action was intentionally omitted in this study to prevent integral windup and preserve a natural, predictable steering feel for the human driver. However, future iterations could explore conditional or low-gain integral control to mitigate long-term steady-state disturbances such as constant crosswinds. Furthermore, for future autonomous driving applications where human steering feel is no longer a constraint, an integral term could be fully utilized to ensure a zero steady-state yaw rate error.

Actuator Delay Compensation via Software Ring Buffer: The current architecture calculates the driver's intended steering angle (δ_{driver}) by subtracting the requested overlay angle from the physically measured road wheel angle. However, due to the mechanical actuation delay of the steering system (50 ms), subtracting the instantaneous overlay request from the delayed physical measurement creates a temporal mismatch. At higher frequencies, this phase error generates a mathematical "ghost signal" that destabilizes the reference calculation and limits the maximum stable proportional gain. Future work should implement a dynamic software buffer to delay the overlay request by the exact duration of the actuator latency before the subtraction occurs. This temporal synchronization would more accurately isolate the true driver intention and increase the system's stability margin.

Bibliography

[1] S. A. Mortazavizadeh, A. Ghaderi, M. Ebrahimi, and M. Hajian, "Recent developments in the vehicle steer-by-wire system," *IEEE Transactions on Transportation Electrification*, vol. 6, no. 3, pp. 1226–1235, 2020. DOI: 10.1109/TTE.2020.3004694.

[2] R. Rajamani, *Vehicle dynamics and control*. Springer New York, NY, 2012, p. 38.

[3] L. Ljung, T. Glad, and A. Hansson, *Modeling and identification of dynamic systems*, 2nd ed. Studentlitteratur, 2021, p. 484, ISBN: 9789144153452. [Online]. Available: https://libris.kb.se/bib/hwzffs11f6b9jj2v.

[4] S. I. for Standards, "Passenger cars — steady-state circular driving behaviour—open-loop test methods," Swedish Institute for Standards, Stockholm, Sweden, Standard SS-ISO 4138, 2021.

[5] S. I. for Standards, "Road vehicles – lateral transient response test methods – open loop test methods," Swedish Institute for Standards, Stockholm, Sweden, Standard SS-ISO 7401, 2011.

[6] A. Rodríguez Sánchez, R. Salmerón Gómez, and C. García, "The coefficient of determination in the ridge regression," *Communications in Statistics: Simulation and Computation*, vol. 51, no. 1, pp. 201–219, 2022, Cited by: 29. DOI: 10.1080/03610918.2019.1649421. [Online]. Available: https://www.scopus.com/inward/record.uri?eid=2-s2.0-85074016199&doi=10.1080%2f03610918.2019.1649421&partnerID=40&md5=73a2e831ba7d9abee1e46c7cb218fe57.

[7] R. H. Shumway and D. S. Stoffer, *Time Series Analysis and Its Applications, With R Examples* (Springer Texts in Statistics), 5th ed. Cham: Springer, 2025, p. 221, ISBN: 978-3-031-70584-7. DOI: 10.1007/978-3-031-70584-7. [Online]. Available: https://doi-org.proxy.lib.chalmers.se/10.1007/978-3-031-70584-7.

[8] L. Ljung and The MathWorks, Inc., *System identification toolbox™ user's guide*, The MathWorks, Inc., Natick, MA, USA, 2025. [Online]. Available: https://www.mathworks.com.

[9] L. Ljung, *System Identification: Theory for the User*, 2nd. Upper Saddle River, NJ: Prentice Hall PTR, 1999.

[10] A. Artuñedo, M. Moreno-Gonzalez, and J. Villagra, "Lateral control for autonomous vehicles: A comparative evaluation," *Annual Reviews in Control*, vol. 57, p. 100 910, 2024, ISSN: 1367-5788. DOI: https://doi.org/10.1016/j.arcontrol.2023.100910. [Online]. Available: https://www.sciencedirect.com/science/article/pii/S1367578823000743.

[11] I. Andrianov and A. Shatrov, "Padé approximants, their properties, and applications to hydrodynamic problems," *Symmetry*, vol. 13, p. 1869, Oct. 2021. DOI: `10.3390/sym13101869`.

[12] Z.-c. Zhao, Z.-y. Liu, and J.-g. Zhang, "Imc-pid tuning method based on sensitivity specification for process with time-delay," *Journal of Central South University of Technology*, vol. 18, no. 4, pp. 1153–1160, 2011, ISSN: 1993-0666. DOI: `10.1007/s11771-011-0817-0`.

A

Appendix 1

A.1 Subjective Evaluation Questionnaire

Gravel Test

Strongly disagree (1) – Strongly agree (7)

1. The active controller significantly reduced the amount of manual counter-steering/corrections compared to open loop.

1	2	3	4	5	6	7

2. The active controller felt intuitive and worked with me; it did not fight against my steering input.

1	2	3	4	5	6	7

3. I preferred:
    - ◯ No Controller Active
    - ◯ Controller Active
    - ◯ Don't Know

4. Any comments or thoughts about the controller performance:

Trailer Driving

Skip questions that don't apply to you
Strongly disagree (1) – Strongly agree (7)

5. The active controller significantly reduced the amount of manual corrections compared to open loop (only answer if you drove with the trailer).

1	2	3	4	5	6	7

6. I felt less disturbances on the vehicle with the controller compared to without controller (for both drivers and passengers).

1	2	3	4	5	6	7

7. The car felt more stable compared to an open loop.

1	2	3	4	5	6	7

8. The controller's interventions were smooth, without any mechanical judder or sudden jerks.

1	2	3	4	5	6	7

9. I preferred:
   - ◯ No Controller Active
   - ◯ Controller Active
   - ◯ Don't Know

10. Any comments or thoughts you would like to share about the controller performance in the trailer test.

Lane Change

Skip this section if you didn't participate in this test
Strongly disagree (1) – Strongly agree (7)

11. While the controller was active, the vehicle quickly stabilized after rapid steering inputs without exhibiting unwanted oscillations or sliding.

1	2	3	4	5	6	7

12. The active controller felt intuitive and worked with me; it did not fight against my steering input.

1	2	3	4	5	6	7

13. The controller's interventions were smooth, without any mechanical judder or sudden jerks.

1	2	3	4	5	6	7

14. The car felt more stable compared to an open loop.

1	2	3	4	5	6	7

15. I preferred:
    - ◯ No Controller Active
    - ◯ Controller Active
    - ◯ Don't Know

16. Any comments or thoughts you would like to share about the controller performance in the lane change test.

DEPARTMENT OF SOME SUBJECT OR TECHNOLOGY
CHALMERS UNIVERSITY OF TECHNOLOGY
Gothenburg, Sweden
www.chalmers.se

AVANCEZ
1829

CHALMERS
UNIVERSITY OF TECHNOLOGY